Dissertation presented to the the University of Twente and Instituto Tecnológico de Aeronáutica, in partial fulfillment of the requirements for the Double Degree programme of Master of Science in the Graduate Program of Mechanical Engineering (UT) & Aeronautical and Mechanical Engineering (ITA), Field of Maintenance Engineering and Operations (UT) & Aeronautical Design, Aerospace Systems and Structures (ITA).

Samuel Franciscus Zijp

REMAINING USEFUL LIFE ESTIMATION FRAMEWORK FOR MAINTENANCE IMPROVEMENT OF A HELICOPTER MAIN ROTOR SHAFT USING FRACTURE MECHANICS

Dissertation approved in its final version by signatories below:

Prof. Dr. A. Nabarette

Advisor

Dr. A. Martinetti

Co-advisor

Prof. Dr. E. Villani

Pro-Rector of Graduate Courses ITA

Prof. Dr. C.H. Venner

Chair exam committee UT

Campo Montenegro
São José dos Campos, SP - Brazil
March 2023

Universtity of Twente graduation number: 424

Cataloging-in Publication Data
Documentation and Information Division

Zijp, Samuel Franciscus
Remaining useful life estimation framework for maintenance improvement of a helicopter main rotor shaft using fracture mechanics / Samuel Franciscus Zijp.
São José dos Campos, 2023.
78p.

Dissertation of Master of Science – Course of Mechanical Engineering (UT) & Aeronautical and Mechanical Engineering (ITA). Area of Maintenance Engineering and Operations (UT) & Aeronautical Design, Aerospace Systems and Structures (ITA) – Instituto Tecnológico de Aeronáutica, 2023. Advisor: Prof. Dr. A. Nabarette (ITA). Co-advisor: Dr. A. Martinetti (UT).

1. Remaining useful life. 2. Aircraft maintenance. 3. Fracture mechanics. 4. Helicopter main rotor shaft. 5. Crack propagation. I. Instituto Tecnológico de Aeronáutica. II. Remaining useful life estimation framework for maintenance improvement of a helicopter main rotor shaft using fracture mechanics.

BIBLIOGRAPHIC REFERENCE

ZIJP, Samuel Franciscus. **Remaining useful life estimation framework for maintenance improvement of a helicopter main rotor shaft using fracture mechanics**. 2023. 78p. Dissertation of Master of Science – Instituto Tecnológico de Aeronáutica, São José dos Campos.

CESSION OF RIGHTS

Samuel Franciscus Zijp
Rua Tenente Benedito Dias Pereira 121, Ap. 13
12227-760 – São José dos Campos–SP

REMAINING USEFUL LIFE ESTIMATION FRAMEWORK FOR MAINTENANCE IMPROVEMENT OF A HELICOPTER MAIN ROTOR SHAFT USING FRACTURE MECHANICS

Samuel Franciscus Zijp

Thesis Committee Composition:

Prof. Dr.	R.T.L. Ferreira	Chairman ITA	-	ITA
Prof. Dr.	C.H. Venner	Chairman UT	-	University of Twente
Prof. Dr.	A. Nabarette	Advisor	-	ITA
Dr.	A. Martinetti	Co-advisor	-	University of Twente
Prof. Dr.	M.A. Arbelo	Internal member	-	ITA
Dr.	R. Loendersloot	External member	-	University of Twente

ITA

Acknowledgments

This thesis is the final work to complete the Double Degree programme of the master Mechanical Engineering at the University of Twente (UT) in the Netherlands and Engenharia Aeronáutica e Mecânica at Instituto Tecnológico de Aeronáutica (ITA) in Brazil. For the past year I have been working on this thesis in Brazil, leaving behind the Netherlands, the UT and friends and family. But it was worth every little bit and therefore I want to thank everyone that was part of this amazing experience!

To start, I would like to thank both my supervisors, Prof. Airton Nabarette and Alberto Martinetti. The experience and knowledge from Prof. Airton Nabarette, ITA supervisor, helped me a lot to reach this final result. Every meeting and discussion about helicopters, my research and Brazil was very useful. Also Alberto Martinetti, my UT supervisor and coordinator of my Master's specialization, was of great importance in reaching this result. Without him I would not have participated in the Double Degree programme. He suggested the programme and helped a lot with organising this adventure.

Furthermore, I would like to thank all the people that made it possible for me to participate in the Double Degree programme. With a special thanks to Marijke Stehouwer, for helping and finding all the right people I needed to make it happen. From the ITA side, I want to thank Mariano Arbello for the courses on fatigue and fracture mechancis, but especially for all the help and random things that needed to be arranged for the UT, ITA or Brazil.

Next, I would like to thank all my friends from Elefante Branco and São José dos Campos. All these people contributed to the great time I had, thank you all! Some names need to be mentioned in particular. First of all Philipe, my roommate, who took me in, showed me ITA and São José dos Campos and helped me with all the practical stuff. Also Sergio, thanks for all the travels, sports, beers and cachaça.

Special thanks to my very good friends in Vinhedo, Ana Paula and Carlos. Thanks a lot for offering me a second home here in Brazil. And of course my parents, for the confidence, support and eventually making this all possible.

Abstract

This research aims to make the next step from diagnostics towards prognostics, using the Health and Usage Monitoring System (HUMS) in combination with fracture mechanics to determine the Remaining Useful Life (RUL) of a helicopter main rotor shaft. This main rotor shaft transfers the power delivered by the engine and the main gear box to the main rotors. At the moment, maintenance to this shaft is carried out after a fixed amount of time, resulting in unused potential. The RUL predictions are used to improve this maintenance strategy and are based on the crack propagation of the main rotor shaft. A framework for these RUL estimations is created using a combination of stochastic, deterministic and statistical calculations. Three main loading types are used as input for the crack propagation calculations: axial, bending and moment loading. Probability density functions (PDF) of these loads are created and used as stochastic load input. A relation is found between the load, crack geometry and stress intensity factor (SIF). This SIF is obtained by modeling the cracked main rotor shaft in the finite element program Abaqus. The relation between the load, crack geometry and SIF is then used to calculate the crack growth rate deterministically using the Walker modification on the Paris' law and Irwin's model. The crack growth rate is calculated for different stress levels during flights. Each flight consists of different stress levels, based on the Felix/28 standard in combination with the PDF stochastic load input. Using this crack growth rate, the crack propagation during flights is determined and so-called degradation paths are constructed. Using the Monte Carlo method, multiple degradation paths are simulated and the RUL is estimated statistically. At last, this RUL estimation is used for maintenance purposes, like determining the inspection interval and plan and anticipate maintenance scenarios. But also putting this framework into the bigger picture of Reliability-Centered Maintenance (RCM).

List of Figures

FIGURE 1.1 – (a) The EC225 Helicopter (SEAFORCES, 1999) and (b) the EC225 Main Rotor Head of the 2016 accident (AEROSSURANCE, 2018) . . . 15

FIGURE 1.2 – Outline of thesis, with indication what chapter contains what topic and which research question is answered where 18

FIGURE 2.1 – General helicopter components (FAA, 2019) 19

FIGURE 2.2 – (a) Picture of a helicopter main rotor head and (b) a schematic representation, in which number 2 indicates the main rotor shaft . . 20

FIGURE 2.3 – Accelerometer on the shell of the MGB of the EC225 (EUROCOPTER, 2012) 21

FIGURE 2.4 – Prognostic method types by (HINES; USYNIN, 2008) 24

FIGURE 2.5 – Prognostic model of degradation paths using the Monte Carlo method, used for RUL estimations (RANDALL, 2011) 25

FIGURE 2.6 – Typical fatigue crack growth behaviour of metals (ANDERSON, 2005) 27

FIGURE 3.1 – Flowchart of RUL calculation procedure 30

FIGURE 3.2 – The three loading modes that can be applied to a crack (ANDERSON, 2005) 33

FIGURE 4.1 – Flowchart for determining the RUL based on crack propagation . . 36

FIGURE 4.2 – Schematic representation of the main rotor shaft configuration . . . 37

FIGURE 4.3 – EC225 helicopter dimensions (AIRBUS, 2015) 38

FIGURE 4.4 – In Abaqus modelled shaft, used for the analysis 39

FIGURE 4.5 – Visualisation of the deformed shaft (scaled), isometric (a) and side (b) view. With clearly visible stress concentration at red areas . . . 40

FIGURE 4.6 – Loading sequence based on the Felix/28 standard (EDWARDS; DARTS, 1984) 42

FIGURE 4.7 – PDF of the different load inputs: (a) Weibull distribution for axial loading, (b) and (c) Normal distribution for bending load and moment load respectively. 43

FIGURE 4.8 – Abaqus crack propagation simulation using XFEM, for visualisation of propagation behaviour. Propagation: (a) Initial crack of 1 mm, (b) intermediate crack propagation and (c) final stage crack propagation 45

FIGURE 4.9 – Abaqus simulation results of (a) the initial crack of 1 mm and (b) a crack of 10 mm (1 mm initial crack and 4.5 mm on both sides) under an angle of 9.58 degrees 46

FIGURE 4.10 –SIF $[MPa/\sqrt{mm}]$ as function of load $[N]$ and crack size $[mm]$ for axial loading. For the SIF mode I or II (K1 and K2) and both crack side (C1 and C2) 47

FIGURE 4.11 –The degradation path of one shaft (a) and multiple shafts (b) from crack initiation to failure. In which the crack size is plotted against the number of flight cycles. 48

FIGURE 5.1 – (a) Monte Carlo simulation of degradation paths and (b) histogram on time to failure data 50

FIGURE 5.2 – Degradation paths and corresponding Weibull distribution, (a) normal view, (b) zoomed in view 51

FIGURE 5.3 – Degradation paths with periodic inspection intervals, indicated by the vertical black lines 52

FIGURE 5.4 – New simulation after crack of 4 mm was found during inspection, degradation paths on the left 53

FIGURE 5.5 – New simulation after crack of 4 mm was found during inspection, with 5% reduction of the total load 53

FIGURE 5.6 – Degradation paths of different loading amplitudes (in percentage of the in Section 4.2.2 specified load), indicated in the graph 54

FIGURE 5.7 – Change in RUL for different loading amplitudes 55

FIGURE 5.8 – Degradation paths of both high and low variance load input distributions. With in red the distribution of the RUL 56

FIGURE 5.9 – Change in RUL for different loading sequence, indicating rough, normal and calm flight cycles 57

FIGURE 5.10 –Degradation paths for Ti-6Al-4V and AISI 4340 58

FIGURE A.1 –Fatigue-crack-propagation data for Ti-6Al-4V titanium alloy (FAA, 2013) 69

FIGURE B.1 –Load diagram for axial loading 72

FIGURE B.2 –Load diagram for bending 73

FIGURE B.3 –Load diagram for moment 74

FIGURE F.1 –RUL (a) and Standard Deviation (b) results from the model for different number of iterations 78

List of Tables

TABLE 4.1 – Material properties of Titanium Ti-6Al-4V and AISI 4340 Steel . . . 39

TABLE 4.2 – Loading combinations and propagation angle for both crack ends (MERR direction) 44

TABLE C.1 – Sequence of loads for each manoeuvre based on Felix/28 (EDWARDS; DARTS, 1984) 75

TABLE D.1 – SIF's at baseline load of 1000 N for axial and bending and 1000 Nmm moment loading 76

TABLE D.2 – SIF's at load of interest for axial, bending and moment loading . . . 76

TABLE D.3 – Comparison of calculated K_I and K_{II} values and Abaqus results . . 76

TABLE E.1 – SIF's for every crack length $[mm]$ per baseline load for mode I or II (K1 and K2) and both crack sides (C1 and C2) [MPa/$\sqrt{mm}$] for Ti-6Al-4V 77

TABLE E.2 – SIF's for every crack length $[mm]$ per baseline load for mode I or II (K1 and K2) and both crack sides (C1 and C2) [MPa/$\sqrt{mm}$] for AISI 4340 stainless steel 77

List of Abbreviations and Acronyms

CBM	Condition Based Maintenance
CI	Condition Indicator
EASA	European Union Aviation Safety Agency
HI	Health Indicator
HUMS	Health and Usage Monitoring System
MGB	Main Gearbox
MTBF	Mean Time Between Failures
MTTF	Mean Time To Failure
MTTR	Mean Time To Repair
PDF	Probability Density Function
RCM	Reliability-Centered Maintenance
RUL	Remaining Useful Life
SIF	Stress Intensity Factor
TBM	Time Based Maintenance

List of Symbols

a	Crack length
C_0	Material constant for Walker equation (when R = 0)
E	Elastic modulus
K	Stress intensity factor (SIF)
K_{Ic}	Fracture toughness
K_{th}	SIF threshold value
m	Material constant for Walker equation
N	Number of cycles
R	Stress ratio
$\frac{da}{dN}$	Crack growth rate
β	Weibull shape parameter
γ	Material constant for Walker equation
η	Weibull scale parameter
ν	Poisson's ratio
σ	Standard deviation
σ_0	Yield strength
σ_u	Ultimate strength

Contents

1 Introduction 15

1.1 Motivation 16

1.2 Research questions 17

1.3 Outline 18

2 Literature Review 19

2.1 Helicopter main rotor shaft 19

2.2 Health and Usage Monitoring System (HUMS) 20

2.3 Maintenance management 21

2.3.1 Reliability-Centered Maintenance 22

2.4 Processing, detection and diagnostic techniques 22

2.4.1 Detection 22

2.4.2 Diagnostics 23

2.5 Prognostic techniques 24

2.6 Fatigue cracking 26

2.6.1 Crack growth rate 26

2.6.2 Computational software 27

2.7 Fatigue crack growth procedures 28

2.8 Stiffness change 28

2.9 Literature overview 29

3 RUL estimation framework 30

3.1 Crack characteristics from Abaqus 31

3.2 SIF to crack growth rate 31

3.3 Mixed-mode loading and the SIF . . . 33
3.4 Crack propagation direction . . . 34
3.5 Degradation paths . . . 34
3.6 Failure threshold value . . . 34
3.7 RUL estimation . . . 35

4 Crack propagation in the EC225 main rotor shaft . . . 36
4.1 Main rotor shaft model . . . 37
4.1.1 Shaft configuration and dimensions . . . 37
4.1.2 Material properties . . . 38
4.1.3 Abaqus model . . . 39
4.1.4 Crack location . . . 40
4.2 Load input . . . 40
4.2.1 Loading assumptions . . . 40
4.2.2 Load specification . . . 41
4.2.3 Loading sequence . . . 41
4.2.4 Probability Density Function (PDF) of loading inputs . . . 42
4.3 Relation between SIF, load and crack length . . . 43
4.3.1 Load change and SIF . . . 43
4.3.2 Geometry change and SIF . . . 44
4.3.3 Abaqus output . . . 46
4.3.4 SIF as function of load and crack length . . . 46
4.4 Crack propagation and degradation paths . . . 47

5 Maintenance improvement . . . 49
5.1 MTTF and RUL . . . 49
5.2 Maintenance planning and RUL . . . 51
5.2.1 Inspection interval . . . 51
5.2.2 Maintenance scenario's . . . 52
5.3 Variability influence . . . 54
5.3.1 Loading amplitude variability . . . 54

5.3.2 Loading input distribution variability 55
5.3.3 Loading sequence variability 56
5.3.4 Material change 57
5.4 RUL and RCM 58

6 Conclusions 60
6.1 Limitations 61
6.2 Future work 62

Bibliography 64

Appendix A – Walker equation constants for Titanium Ti-6Al-4V 69

Appendix B – Load diagrams 72
B.1 Load diagram: Axial load 72
B.2 Load diagram: Bending load 73
B.3 Load diagram: Moment load 74

Appendix C – Felix standard for loading sequence 75

Appendix D – Mathematical explanation: Load change and SIF 76

Appendix E – Abaqus output 77

Appendix F – Monte Carlo simulation iterations 78

1 Introduction

The model EC225 Helicopter was announced by Eurocopter in June 1998, certified airworthy in 2004 (EASA, 2021) and still produced today by Airbus. A picture of this helicopter is shown in Figure 1.1a. Over the years accidents have happened with this helicopter. On February 18, 2009 an EC225 Helicopter ditched in the sea while approaching an offshore oil platform, all passengers onboard were rescued (AAIB, 2011). In 2012 two helicopters were forced to perform a controlled landing into the North Sea, after a warning indicated a failure of the emergency lubrication system (AAIB, 2014). In both cases, the bevel gear vertical shaft in the main rotor gearbox had failed. Both emergency landings were successful and the crew and passengers were rescued. However, on April 29, 2016 another EC225 Helicopter crashed and all 13 passengers on board perished (AIBN, 2018). The cause of this crash was the detachment of the main rotor assembly of the helicopter, which was caused by a gear failure in the main gearbox (MGB). The main rotor head of this accident is shown in Figure 1.1b.

(a) (b)

FIGURE 1.1 – (a) The EC225 Helicopter (SEAFORCES, 1999) and (b) the EC225 Main Rotor Head of the 2016 accident (AEROSSURANCE, 2018)

The 2009 accident can be attributed to human error. However, the other three accidents were caused by system failure, of the MGB in particular. According to the investigation report on the 2016 crash (AIBN, 2018), the gear failure occurred in a way that could not have been detected by the maintenance procedures or monitoring systems at the time of the accident. After this crash, measures were taken by various parties, including the European Union Aviation Safety Agency (EASA), to enhance safety (EASA, 2018). Some of the safety measures included better fatigue evaluation and condition monitoring.

An example of a condition monitoring system is the Health and Usage Monitoring System (HUMS). The term HUMS dates back to 1985 (LAND, 2001) and since then a lot of research is done on these monitoring systems. The HUMS records the condition of critical systems and components in helicopters, making it possible to detect progressive defects or early indications of them. By doing so, suitable actions can be taken in a way to mitigate potential risks to operational safety (SKYBRARY, n.d.). From a maintenance point of view, the HUMS is also very interesting. The HUMS makes it possible to perform Condition Based Maintenance (CBM), minimizing, for example, the maintenance downtime by better maintenance planning.

The goal of this research is to improve maintenance management of the EC225 Helicopter, making use of the HUMS. The HUMS will be used to make the next step from diagnostics towards prognostics, which in turn is used to improve maintenance management. The Remaining Useful Life (RUL) plays an important role in this maintenance management as well. Better RUL estimations, will help with better maintenance decisions, which can help with increasing the useful life of the system.

1.1 Motivation

Maintenance of critical systems and parts is important to keep a system operational, also for the Eurocopter EC225. At the moment, maintenance tasks for the EC225 are carried out after at least 735 flying hours (AIRBUS, 2021), this is known as Time Based Maintenance (TBM). Typically, maintenance to shafts is done at the same time the MGB is overhauled, which is every 2000 flying hours for the EC225 helicopter (AAIB, 2014). However, in most cases maintenance is not yet required after this fixed amount of flight hours and potential is unused. Optimized maintenance strategies, like CBM, can ensure optimum utilization of the helicopter and its components. CBM has been used for a long time in the so called HUMS for safety and optimization purposes, but more optimization is definitely possible.

It is known that CBM and HUMS are necessary for monitoring the helicopter rotor system and its subsystems. The EC225 contains many different components that need monitoring, some more critical than others. One of the more critical components is the main rotor shaft, which is the main focus of this research. The main rotor shaft transfers the power delivered by the engine and the MGB to the main rotors. This shaft is a rotating component, which can fail due to unbalance, misalignment and wear. As mentioned before, failure can have catastrophic consequences and should be prevented. Reliable RUL predictions can contribute to this prevention. More reliable predictions on the lifetime of the main rotor shaft and better maintenance management can help extend

the time to maintenance, reduce costs and make the life-cycle efficient.

This research focuses on maintenance optimization of the main rotor shaft, taking into account CBM, HUMS and RUL. A new way of working is proposed, combining different disciplines to achieve more reliable RUL predictions. These predictions are made using a combination of stochastic, deterministic and statistical calculations, based on rotor dynamics and fracture mechanics. The aim is to create a step by step approach or framework, considering these different disciplines for RUL predictions for the main rotor shaft of a helicopter. The model EC225 Helicopter will be used for creating and evaluating the framework.

1.2 Research questions

The main research question that will be answered in this thesis is:

"How could the overall useful life of the EC225 main rotor shaft be improved using a combination of the HUMS and RUL estimations?"

This main research question will be answered using the following sub-questions:

1. *How can the HUMS contribute to RUL estimations?*
2. *How can the RUL of the EC225 main rotor shaft be estimated?*
3. *What maintenance management benefits can be achieved with reliable RUL estimations?*

1.3 Outline

Answers to the research questions are found throughout this report and given in the conclusion at the end of this report. Figure 1.2 shows a schematic overview of the outline of the thesis. In this schematic overview it is indicated which research question is answered in which chapter. The research starts with the introduction and the research questions, given in the chapters above. In upcoming chapter, a literature review is presented on current technologies regarding for example HUMS, CBM and RUL. A brief summary of the literature review is given in Section 2.9, also explaining decisions made for this research. After that, the RUL estimation framework is discussed. Explaining how the RUL is estimated and what important assumptions have been made. This framework is then validated by and used to obtain degradation paths for the EC225 main rotor shaft in Chapter 4. RUL estimations on this EC225 main rotor shaft are done in Chapter 5. This chapter also discusses how the RUL estimations can be used for maintenance improvement. The report ends with the conclusions and recommendations, limitations of the research and possible future work.

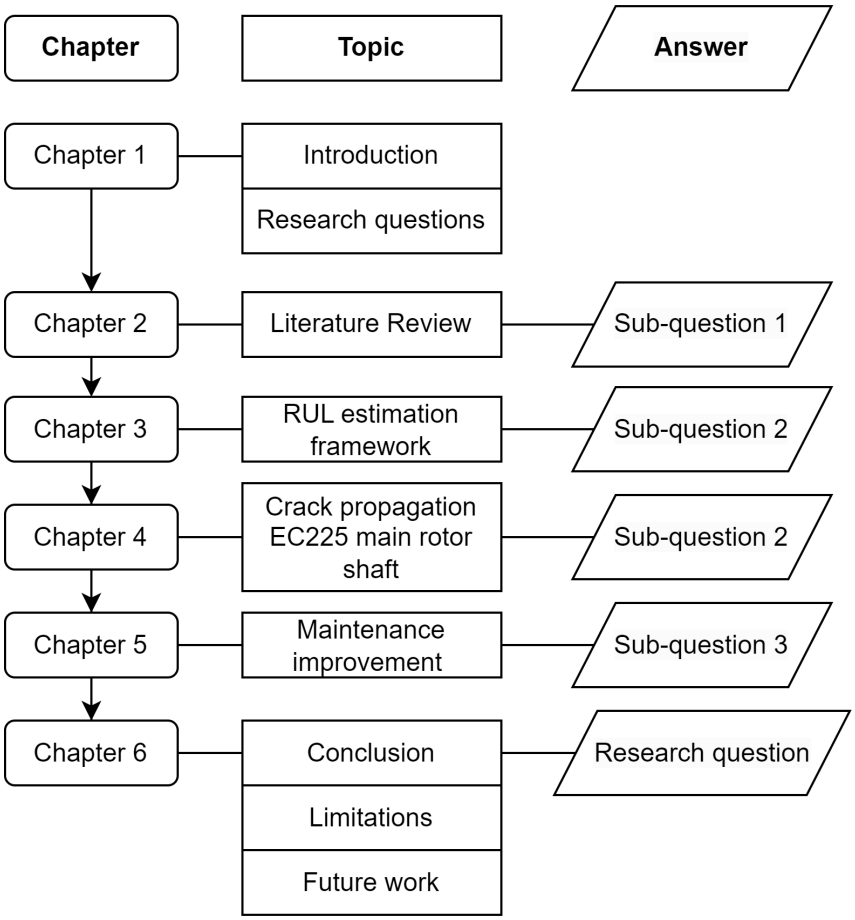

FIGURE 1.2 – Outline of thesis, with indication what chapter contains what topic and which research question is answered where

2 Literature Review

This chapter gives a literature review on subjects relevant for this research. Starting with the helicopter main rotor shaft itself and the HUMS. Also maintenance management, diagnostic and prognostic techniques and fatigue cracking is discussed. This chapter ends with a brief summary on the literature review.

2.1 Helicopter main rotor shaft

The main components of a helicopter are the airframe, fuselage, landing gear, engine, MGB, main rotor system and tail rotor system. These parts are schematically shown in Figure 2.1. As stated earlier, this research will focus on the main rotor system, with in particular the main rotor shaft. The purpose of the main rotor shaft is to transfer the power delivered by the engine and the main gearbox to the main rotors.

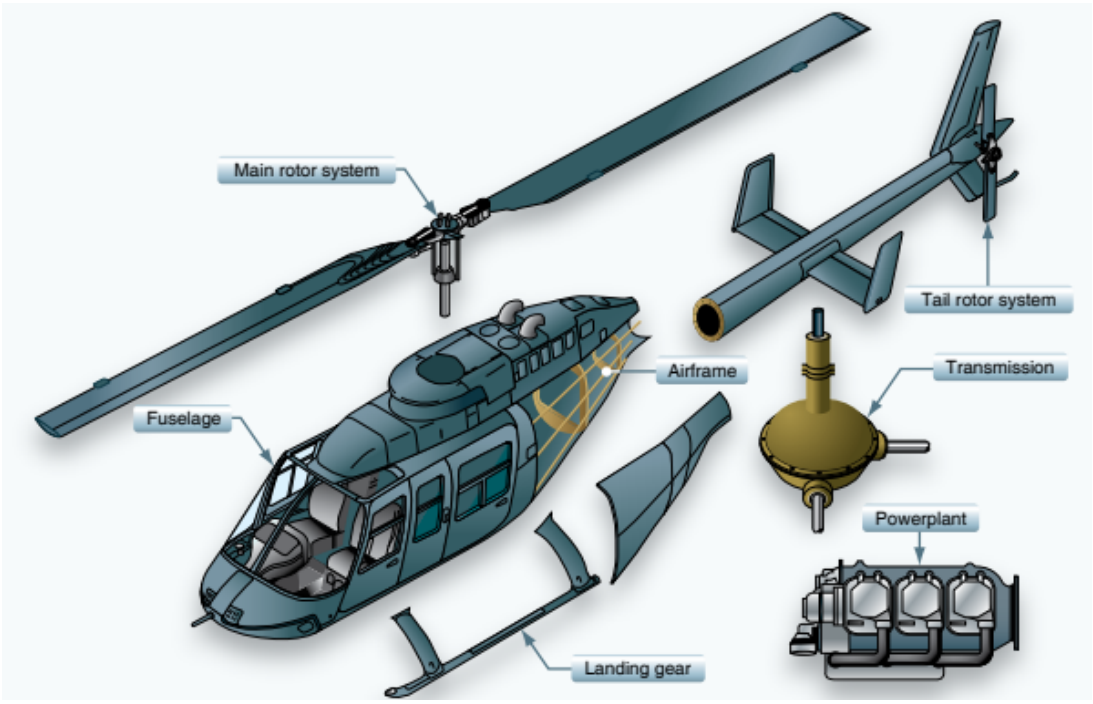

FIGURE 2.1 – General helicopter components (FAA, 2019)

The main rotor shaft is part of the main rotor system. A close-up of this system is given in Figure 2.2a, with in Figure 2.2b a schematic representation of the system. In this schematic representation, number 2 indicates the main rotor shaft.

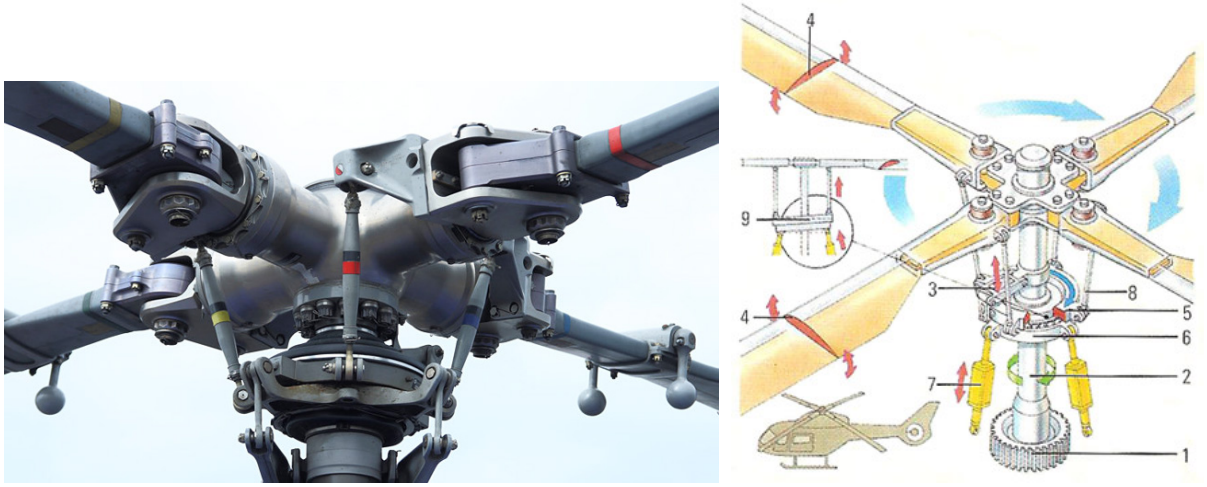

(a) (MCCLELLAN, 2018) (b) (DARLING, 2016)

FIGURE 2.2 – (a) Picture of a helicopter main rotor head and (b) a schematic representation, in which number 2 indicates the main rotor shaft

2.2 Health and Usage Monitoring System (HUMS)

The HUMS is designed to alert the operator of any issues that might compromise the airworthiness of the aircraft (WIIG, 2006). The core of the HUMS is component-vibration monitoring. But also engine monitoring, rotor track and balance and flight-data monitoring is used. More general, the ability to pull flight parameters off the aircraft (SEIDENMAN, 2020).

In most cases the HUMS obtains vibration data from accelerometers present in a helicopter. These accelerometers are not placed directly on the gears or shafts, but for example at the outside of the housing. An example of a HUMS sensor is shown in Figure 2.3. This accelerometer registers all vibrations in its vicinity, from nearby gears, shafts or bearings. The signal contains the accelerometers raw vibration data (EUROCOPTER, 2012).

Just the raw vibration data does not give much information about (possible) failures. Data processing is needed to get useful information from the raw data and is therefore of great importance. For data processing so called condition indicators (CI) are used. These indicators show changes in values, such as increase or decrease, that occur when transitioning from a healthy state to an unhealthy one. What the problem is and how these are found mainly depends on the CI's and how they are described.

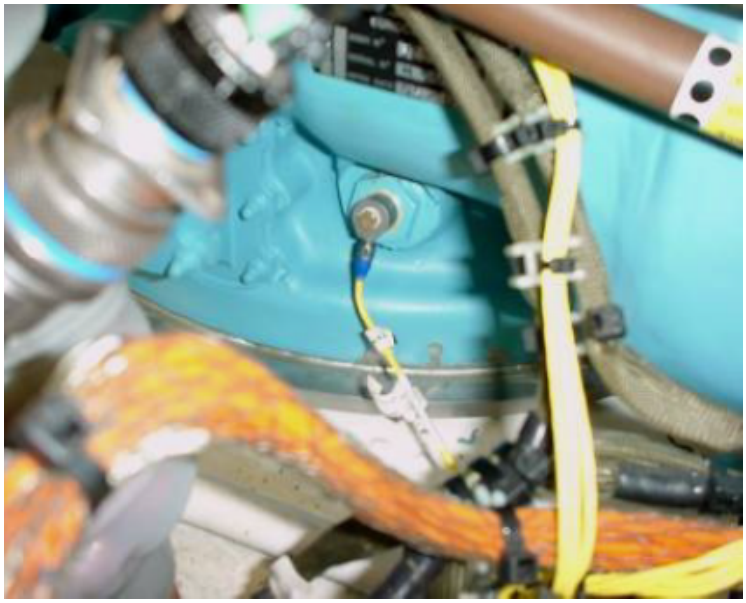

FIGURE 2.3 – Accelerometer on the shell of the MGB of the EC225 (EUROCOPTER, 2012)

2.3 Maintenance management

Within maintenance engineering, a distinction is made between different maintenance types: corrective, preventive and predictive maintenance. Corrective and preventive maintenance are described clearly by Tinga (TINGA, 2010). Corrective maintenance can be seen as the most basic strategy, in which replacement or repair takes place after failure. In this case the whole service life is used, but problems may arise for system availability and safety. With the preventive maintenance strategy, parts or systems are replaced or repaired before they fail, failure is prevented. For this strategy maintenance is carried out periodically, also known as TBM. Predictive maintenance, also known as CBM, is described by Randall (RANDALL, 2011) as maintenance that is carried out at the most optimal moment, because potential breakdown is predicted by condition monitoring.

The HUMS is a good example of a system that is used for system monitoring and data analysis, and therefore closely related to CBM. The HUMS is used to provide information about the flight and the system, which can be used for maintenance purposes. Maintenance tasks can be anticipated by, for example, abnormal vibration levels, indicating cracks or unbalances (EUROCOPTER, 2012). However, the right maintenance task or decision is depending on more factors and it is important to put everything into a bigger picture. Reliability-Centered Maintenance (RCM) is a good example of a maintenance concept to determine which activities need to be taken.

2.3.1 Reliability-Centered Maintenance

RCM integrates various maintenance strategies such as corrective, time-based, interval-based, condition-based and proactive maintenance. The goal of RCM is to increase the probability that a machine or component will operate as required throughout its life-cycle, while minimizing downtime and maintenance costs. The maintenance strategies are combined and their individual benefits are integrated as optimal as possible, thereby maximizing equipment availability and reliability, while minimizing life-cycle costs (NASA, 2008).

Pride (PRIDE, 2016) states that nowadays the role of failure rate or failure frequency is decreasing within maintenance programs. Although failure frequency can be useful for making cost decisions and establishing maintenance schedules, it doesn't provide any information about which maintenance tasks are suitable or what the impact of failure is. To assess a maintenance solution, it's important to consider how it can prevent safety, security, and/or economic consequences. According to the RCM guide (NASA, 2008), ensuring safety and security is of utmost importance, and life-cycle cost is a tertiary criterion.

2.4 Processing, detection and diagnostic techniques

One of the main goals of maintenance engineering is carrying out maintenance at exactly the right moment. Predicting when the failure will occur and preventing it from happening, by carrying out maintenance just before failure. Predicting and preventing is usually done using condition monitoring systems like the HUMS.

Randall explains in his book 'Vibration-based condition monitoring' (RANDALL, 2011) how vibration analysis, and in particular accelerometer signals, play an important role in condition monitoring. It explains the different parts of it; the data itself, signal processing, detection, diagnosis and prognosis. A lot of research is carried out on detection and diagnostic techniques, while relatively little research has been done on prognostic techniques.

2.4.1 Detection

Cracking of the shaft is one of the failures that can have catastrophic consequences for systems. Detection of cracks in shafts is therefore researched frequently. The studies are done for different applications and with different operating conditions. Teyi and Singh made a review on modelling and analysis of cracked rotors from 2010 until 2021 (TEYI;

SINGH, 2022). Many of the studies discussed in this review are focused on using vibration data for detection of cracks.

The research of Gómez et al. discusses examples for using vibration data in existing detection and diagnostic techniques on shaft cracking (GóMEZ *et al.*, 2016). It shows a way of using vibration data for detecting cracks in rotating shafts. Fatigue crack detection is investigated in the research of Prasad and Sekhar, they use different time-frequency analysing techniques for this (PRASAD; SEKHAR, 2020). One of those techniques is continuous wavelet transforms (CWT), researched more in depth by Silva et al. In this research the main goal is early fault detection in gas turbines with accelerometer data processing (SILVA *et al.*, 2020).

There are several other non-destructive testing techniques, including radiography, ultrasonic, magnetic particle, and eddy current testing. However, these methods require prior knowledge of the location of the cracks. Also, the region should be accessible for testing. Following the statement of Kushwaha and Patel, this can be a problem and making vibration-based crack identification methods more useful (KUSHWAHA; PATEL, 2020).

2.4.2 Diagnostics

Diagnostics is the next step after detection, identifying what the failure is. Different techniques and models are researched on this topic as well. Randall gives in his book an overview of available techniques, from harmonic and sideband cursors to spectral kurtosis and the kurtogram (RANDALL, 2011).

Antoni and Randall show in their paper (ANTONI; RANDALL, 2006) the effectiveness of Spectral Kurtosis (SK) in vibration-based condition monitoring of rotating systems. They describe a method in which defects in rotating systems causes a series of impacts that generate transient vibration signals. These signals can then be analysed using different filters.

Methods for failure diagnostics depend on the so-called Health Indicators (HI) or CI's extracted from condition monitoring data, discussed by Atamuradov et al. (ATAMURADOV *et al.*, 2020) and Zhu et al. (ZHU *et al.*, 2014) respectively. There are many different indicators researched, an important one is the harmonics of the signal. This indicator is also discussed in the work of (WIIG, 2006), (EUROCOPTER, 2012), (SCHONENBERG, 2015) and (EVERTS, 2016).

2.5 Prognostic techniques

Condition monitoring contributes to reliable predictions for how long a system or component can operate safely, reliably and/or economically. Condition monitoring also plays an important role in prognostics, in which the RUL predictions is one of the key components. Unfortunately, prognostics is the least developed technique within CBM.

In the review of Heng et al. (HENG *et al.*, 2009) a distinction is made between two types of condition-based predictions, those based on physics and those based on data. Randall (RANDALL, 2011) uses this distinction as well and describes both as follows: Physics-based models rely on a physical or mathematical representation of the failure modes, such as crack growth rates. These models use measurements to estimate the extent to which a particular failure mode has progressed. In contrast, data-based models are developed by analyzing measurement data from historical cases to derive failure models using statistical methods. Another approach for data-based models is to identify features that indicate faults and use trend analysis to predict the progression of these faults. For example when a component deteriorates, a linear or exponential regression can be fitted, based on the measured data. When the wear increases the dynamic load, which increases the wear and so on, an exponential curve will be more suitable. Some of the failure propagation types are also described by Atamuradov et al. (ATAMURADOV *et al.*, 2020). In general, large amounts of data are required for data-driven models. However, simulation models can be used to create data from simulated faults and resolving this problem.

Hines and Usynin (HINES; USYNIN, 2008) define three prognostic method types based on the type of information they use. This approach is described by Randall (RANDALL, 2011) as an 'excellent' approach. Hines and Usynin describe the types as follows: (Type I) Time-to-Failure Data-Based prognostics, (Type II) Stress-Based prognostics and (Type III) Effects-Based prognostics. A schematic representation of the three types defined by Hines and Usynin is given in Figure 2.4.

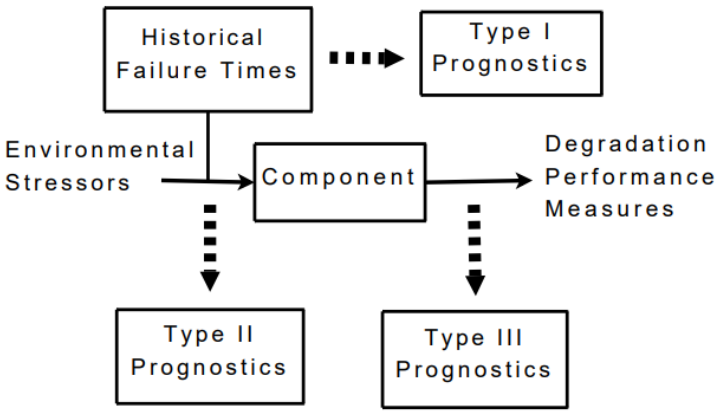

FIGURE 2.4 – Prognostic method types by (HINES; USYNIN, 2008)

Type I prognostics is described as time-to-failure data-based prognostics and is based on historical and statistical data. It provides a failure distribution for the average component operating under average conditions. However, operating conditions can influence the failure distribution. Type II prognostics is the stress-based prognostics, which takes these operating conditions into consideration. And finally Type III, the effect-based prognostics, which is seen as the best approach. Hines and Usynin (HINES; USYNIN, 2008) described the effects-based prognostic type as prognostics that rely on degradation measures to make predictions. These measures are numerical representations of the system's current ability to perform its intended functions accurately. The measures can be expressed as either a scalar or a vector quantity. The probability of failure at any given moment is correlated with these measures. They may not necessarily be directly measured parameters but can be derived from various measured variables, providing a quantitative measure of degradation.

The effect-based prognostics approach (Type III) can be used to create so called degradation paths, which in turn can be used for failure prediction. A good example of those degradation paths is shown in Figure 2.5. It shows a collection of degradation pathways (Monte Carlo method) that progresses towards the failure threshold. If the current level of degradation can be determined through inspections, it is possible to simulate and forecast potential degradation paths from the current state as well. The degradation paths can then be used to create failure distributions of components. These distributions can provide useful information like RUL predictions, which can be used for decision making.

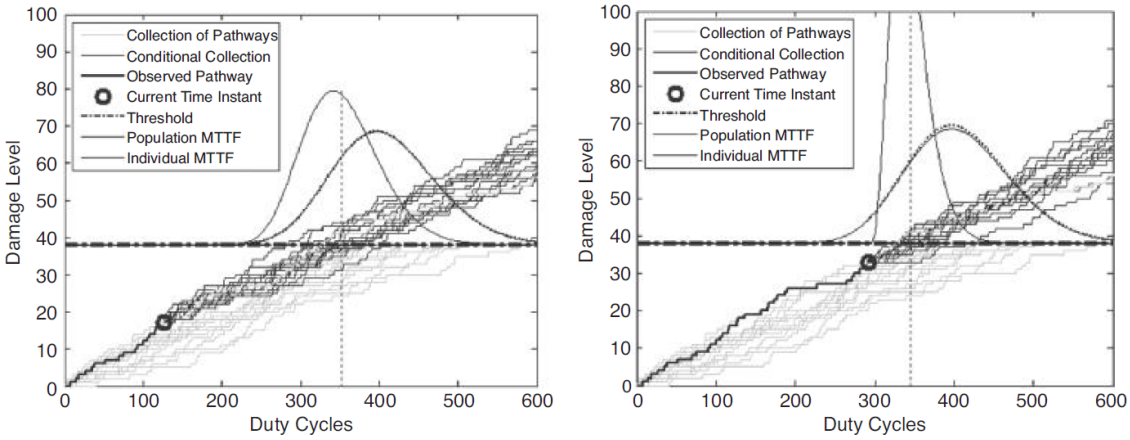

FIGURE 2.5 – Prognostic model of degradation paths using the Monte Carlo method, used for RUL estimations (RANDALL, 2011)

To be able to perform reliable RUL predictions during operations using effects-based prognostic methods, it is important to estimate the current state of degradation. Diagnostic techniques and HI or CI are important for determining this current state. For example changing trends in vibration parameters, for situations like development of imbalance, misalignment and wear. The amount of change in trends needs to be quantified to be able to say something about the current state of the component.

2.6 Fatigue cracking

For creating effects-based degradation plots for main rotor shaft cracking, knowledge about the crack propagation of this shaft is required. Much research is done on cracks in shafts, such as on the Stress Intensity Factor (SIF). The SIF is useful for characterization of the crack, crack propagation and eventually fatigue life calculations of the shaft.

The SIF's can be determined for many different loading types, configurations and crack geometries. Papers can be found on this topic for specific cases, dating back to 1986 (UNDERWOOD *et al.*, 1986). These SIF's can also be created or verified using numerical finite element methods. The research of Khoo and Karuppanan is a good example for analytical and numerical results for SIF's in shafts (KHOO; KARUPPANAN, 2011). Many equations are constructed for numerical determination of the SIF for the different cases, these equations are combined in certain handbooks, like the 'USAF Damage Tolerant Design Handbook: Guidelines for the Analysis and Design of Damage Tolerant Aircraft Structures' (MIEDLAR *et al.*, 2002).

During normal operation of a helicopter, a combination of different loading types and crack geometries will be present. A variable amplitude loading will be present as well, due to the helicopters' operation cycle, including take-off, hovering and landing. This is a complicating factor and needs to be taken into account when analysing the stresses in the shaft. Unfortunately, this makes many researches, that only focus on specific loading cases, unsuitable.

2.6.1 Crack growth rate

The crack is growing during operation at a certain rate per number of cycles, the crack growth rate. This rate is described by da/dN and depends on the SIF. Different methods for calculating this crack growth rate are available in literature. The first person to introduce the idea that the crack growth rate is depending on the SIF is Paris (PARIS *et al.*, 1961), leading to the famous Paris' law. Later more alternatives on this law were developed, like the Forman (FORMAN *et al.*, 1967), Walker (WALKER, 1970), Collipriest (COLLIPRIEST, 1972) and NASGRO (FORMAN *et al.*, 2005) equations.

The fatigue crack growth behaviour of metals is typically described by the graph in Figure 2.6. The curve is divided into three regions: (I) near the threshold, (II) steady state and (III) near instability. In region I, the da/dN approaches zero at a threshold value ΔK_{th}. The crack will not propagate below this threshold value. In region II, the curve is linear and can be described by the famous Paris' law or it's alternatives. And in region III, the ΔK reaches the fracture toughness of the material. At this fracture toughness the crack growth will be unstable and fracture will happen (ANDERSON, 2005).

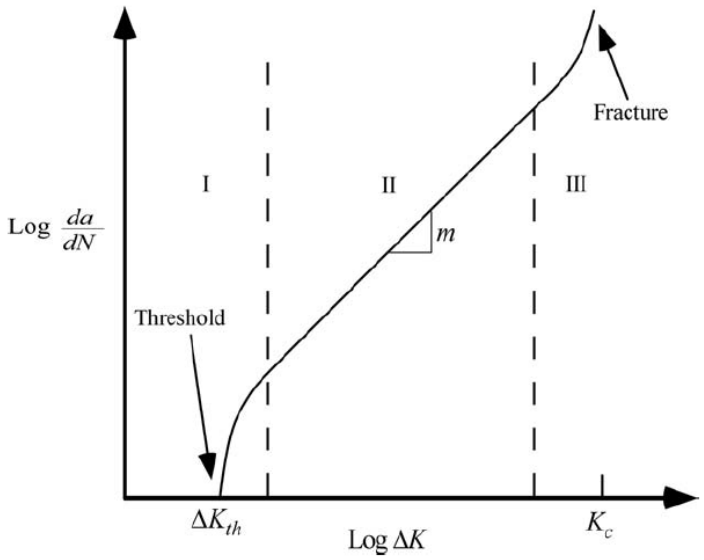

FIGURE 2.6 – Typical fatigue crack growth behaviour of metals (ANDERSON, 2005)

The linear part of the graph (region II) can be described by the Paris equation or its alternatives. In subsequent research, equations have been found to describe multiple regions as well. Like the Forman equation describing regions II and III (FORMAN *et al.*, 1967) or the Collipriest equation that describes all three regions (COLLIPRIEST, 1972).

2.6.2 Computational software

In this thesis a combination of loads and changing geometries during crack propagation are present. This makes it difficult to use available deterministic methods for SIF calculations. However, finite element methods are available and included into computational software.

A good example of the use of computational software is the master thesis of M. Oliveira (OLIVEIRA, 2018). In this research NASGRO software is used to calculate the crack growth. The research of Zhang et al. (ZHANG *et al.*, 2019) shows how the finite element software Abaqus is used in combination with Franc3D, to predict the crack propagation path and the SIF's. Another crack propagation program used in research is AFGROW. In the research of Bordeasu et al. (BORDEASU *et al.*, 2009), ANSYS and AFGROW are used for numerical simulations of fatigue crack initiation and propagation for horizontal axial turbines shafts. And finally Zencrack, Maligno et al. investigated the fatigue crack growth in shafts numerically using this program (MALIGNO *et al.*, 2009).

As already explained earlier in this subsection, the loading of the shaft will be under variable mixed-mode loading conditions. Because of this variable mixed-mode loading, the crack propagation behaviour will develop in a complex 3D way. It might be possible

to do the calculations on the crack propagation deterministic. However, the use of computational software might be better, faster and easier. Using those programs the SIF can be determined, and used for crack propagation.

2.7 Fatigue crack growth procedures

Computational programs can be used to find crack and propagation characteristics. These characteristics are used in different studies to create procedures or algorithms for determining the crack growth process. One of them is the research of Yang and Vormwald (YANG; VORMWALD, 2017), which proposes a procedure for simulating fatigue crack growth under a cyclic mixed mode loading. The procedure consist of three main parts: (1) Identifying the crack initiation location; (2) obtaining the maximum equivalent SIF (K_{eq}) for one cycle; and (3) defining the crack growth process. Repeating steps 2 and 3 will lead to visualisation of the crack growth process.

The study of Yang and Vormwald (YANG; VORMWALD, 2017) focuses on simulation of the crack growth during a cyclic loading, in what way the crack propagates. However, in this thesis the focus will be on fatigue crack growth and the degradation paths. Nevertheless, the way of working discussed in the study can be very interesting.

2.8 Stiffness change

The current state of the shaft and the crack is important for RUL estimations. There are different methods for detecting the crack and diagnosing the current state of the shaft. A mechanical relation between the rotating shaft and the crack growth that might be interesting for this thesis, is the stiffness change. This stiffness change can be seen as a CI.

As a consequence of cracks in a structure is the change of its stiffness. With knowledge of rotor dynamics it can be assumed that a crack in a shaft will cause its stiffness to decrease. In the book of Krämer, 'Dynamics of Rotors and Foundations' (KRAMER, 1993), this principle is explained using a horizontal Jeffcott rotor. The crack breaths under its own weight due to gravitation. The bending of the shaft and the opening and closing of the crack will result in a constantly changing stiffness.

In this thesis, the main rotor shaft is a vertical shaft, so there will be much less gravitational influence on breathing. However, due to other present forces it can be assumed that the stiffness will change during rotation when a crack is present. This will lead to a change in displacement of the shaft and a change in the vibration signal.

The changing stiffness during operation can be described as follows: (1) No crack will be present at the start of using the shaft, so the stiffness will be maximal. (2) Eventually a crack will initiate and the stiffness changes, causing the displacement and vibration to increase. (3) This crack will now have higher stresses and the crack will propagate. (4) Again the stiffness will change, as well as displacement, vibration and cracking. This vicious circle of crack propagation can be used for detection and diagnostics, as well as RUL calculations.

In this section, the stiffness change in relation to the change in vibration data is an interesting characteristic. This vibration data might be analysed using earlier discussed techniques and a relation between crack growth, stiffness change and change in vibration data can be found. Which can be used to verify the crack propagation. A benefit of this principle is that there is no physical inspection needed.

2.9 Literature overview

In the literature review various subjects were discussed, from HUMS to fatigue cracking and from RCM to degradation paths. It shows that a lot of research is done on the individual topics, like diagnostic techniques for cracks in shafts or the SIF of certain crack geometries. However, research on the combination of these topics into a bigger picture is missing. This research will focus on the combination of how different disciplines like rotor dynamics, fracture mechanics and maintenance engineering can be combined for optimizing the maintenance management.

It was shown that stiffness change can be an interesting characteristic to use vibration data for crack diagnostics. Furthermore, it can also be seen that the RUL is a useful tool to quantify the condition of a part or system. A method for obtaining and using this RUL will be one of the main goals of this research. For every possible situation or scenario different models, procedures or approaches are mentioned. Therefore, it is impossible to research and optimize every topic on combining the different disciplines in one master thesis. It is chosen to focus on the crack propagation, RUL estimation and maintenance management.

The component that is researched is the main rotor shaft. And the model EC225 Helicopter will be used for evaluating the proposed framework. Nevertheless, it is important to mention that it might be possible to use this research on and apply it to other components or systems as well. A framework will be created and explained based on the main rotor shaft, but will be applicable to other purposes as well.

3 RUL estimation framework

The main goal of this research is to determine the RUL of the main rotor shaft for maintenance purposes. This will be done using simulation and computational programs. The simulation program is Abaqus and will be used for determining the crack propagation characteristics. The computational program Matlab will be used for the calculations, turning the loading and crack propagation data into useful information.

The RUL is calculated using crack propagation theory from fracture mechanics. To perform these calculations an initial crack size is necessary. It is hard to predict when the initial crack will appear in the shaft, but it is possible to detect when a crack is present. Certain diagnostic techniques, like vibration data and stiffness reduction, can be used for this. The crack characteristics for this initial crack can be found using Abaqus. Subsequently, these characteristics are used in Matlab for calculating the crack growth during one loading cycle, one flight cycle. The crack has changed after this one loading cycle, increased in size, and as a result, the crack characteristics have changed. New crack growth is determined for the next loading cycle. Followed by new crack characteristics and new crack propagation and so on, until the component will fail. This iterative process will create a so called crack growth path or degradation path.

How the crack will propagate depends on variables like the crack itself and the applied load. Therefore, different crack growth scenarios are possible for this iterative process, creating different degradation paths. Simulating many of these degradation paths will give a distribution for RUL calculations. This way of simulating many different possible degradation paths can be seen as the Monte Carlo method. More about this iterative procedure of simulating degradation paths is described in upcoming subsections. The procedure of determining the RUL, as described above, is represented using a flowchart, shown in Figure 3.1.

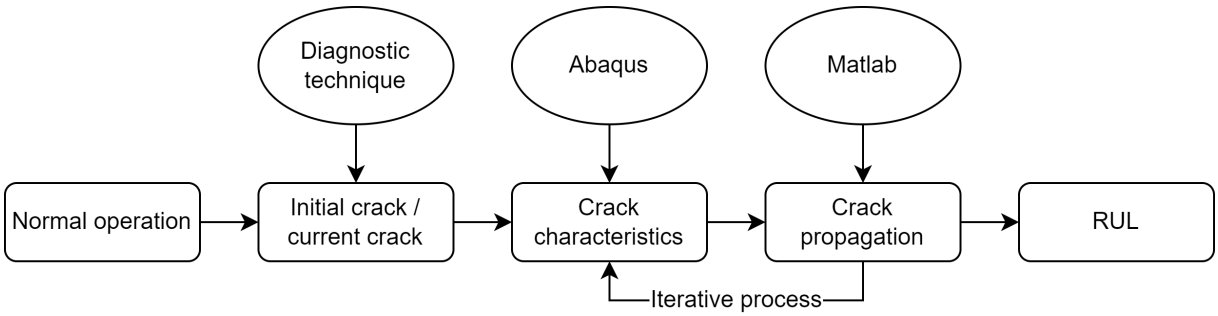

FIGURE 3.1 – Flowchart of RUL calculation procedure

As discussed in Section 2.5, for RUL estimations it is important to know what the current state of the component during operation is. Diagnostic techniques can be of help here. The focus of this research is on the crack and crack propagation towards the RUL. The methods for determining the RUL from the crack characteristics is discussed further in the rest of this chapter .

3.1 Crack characteristics from Abaqus

A model of the main rotor shaft is made in Abaqus, representing the real life situation as much as possible. This model is used to acquire the necessary crack characteristics. The model itself is described in depth in Section 4.1.3.

The fracture mechanics part of Abaqus can provide different types of results. The most interesting characteristic in this research is the SIF, which plays an important role in linear elastic fracture mechanics. It characterizes the stress state at the tip of the crack, which is influenced by both the crack geometry and the applied load. The SIF can be used for determining the crack propagation, discussed further in Section 3.2.

Besides the SIF, Abaqus can be used to determine the crack propagation direction. Abaqus uses three criteria for determining the propagation direction: (1) the maximum tangential stress criterion; (2) the maximum energy release rate criterion (MERR); (3) the K_{II} criterion. In this research the MERR is used, which states that the crack will propagate in the direction with the highest energy release rate.

3.2 SIF to crack growth rate

The RUL for the system is the time the crack will need to propagate until the point of failure, which depends on the crack growth rate. There are different models to determine this crack growth rate. The crack growth rate can be described as the crack propagation per number of cycles, $\frac{da}{dN}$. According to the Paris' Law, the crack growth rate depends on the SIF (PARIS *et al.*, 1961) and the equation looks as follows:

$$\frac{da}{dN} = C(\Delta K)^m \tag{3.1}$$

The C and m in this equation are material constants and ΔK is the SIF range. During one flight cycle, or one repetition, different loads are applied on the shaft, causing the stress ratio R to be non-zero. The Paris equation does not take this R into account. Because of the variable amplitude loading, some adjustments need to be made to the Paris equation of Equation 3.1. Walker suggested a modification to account for this variability.

In this modification the sequence effect is neglected and loading history is not taken into account. The modified equation looks as follows:

$$\frac{da}{dN} = C_0 \left(\overline{\Delta K}\right)^m \tag{3.2}$$

C_0 is the material constant, but in this case corresponding to $R = 0$. This coefficient is used because of the use of $\overline{\Delta K}$, which accounts for the different R-ratios. The $\overline{\Delta K}$ is defined as:

$$\overline{\Delta K} = \frac{\Delta K}{(1-R)^{1-\gamma}} \tag{3.3}$$

Where γ is a material constant as well and ΔK and R are determined by:

$$\begin{aligned} \Delta K &= K_{max} - K_{min} \\ R &= \frac{K_{min}}{K_{max}} \end{aligned} \tag{3.4}$$

So the crack growth rate can be determined using:

$$\frac{da}{dN} = C_0 \left[\frac{\Delta K}{(1-R)^{1-\gamma}}\right]^m \tag{3.5}$$

This formula calculates the crack growth rate for a constant amplitude loading with constant non-zero R. However, during one flight cycle of the helicopter there is a variation in the stresses, SIF's and R. To calculate the crack growth during one flight cycle, the crack growth for each individual cycle within one flight cycle needs to be determined. This can be done using Equation 3.5 and the fact that for one cycle $\Delta N = 1$. So the crack growth of one cycle is given by:

$$\Delta a = C_0 \left[\frac{\Delta K}{(1-R)^{1-\gamma}}\right]^m \tag{3.6}$$

Summing this for all individual cycles, within one flight cycle, gives:

$$\Delta a_B = \sum_{j=1}^{N_B} \Delta a_j = \sum_{j=1}^{N_B} C_0 \left[\frac{\Delta K_j}{(1-R_j)^{1-\gamma}}\right]^m \tag{3.7}$$

With this equation the crack growth during one flight cycle can be calculated. The SIF's during every individual cycle is important in this equation, as it is the only actual variable.

3.3 Mixed-mode loading and the SIF

As discussed in the previous section, the SIF is important. The SIF depends on the load and stresses around the crack tip. In this research, the shaft is subjected to three loading types: (1) Axial load; (2) Bending; (3) Moment or torque. More about these types is discussed in Section 4.2.1. However, these types of loading have their influence on the load and stress at and around the crack tip. The crack tip can experience three different types of loading. These different modes, as they are called, also have their own SIF. The three different modes are shown in Figure 3.2.

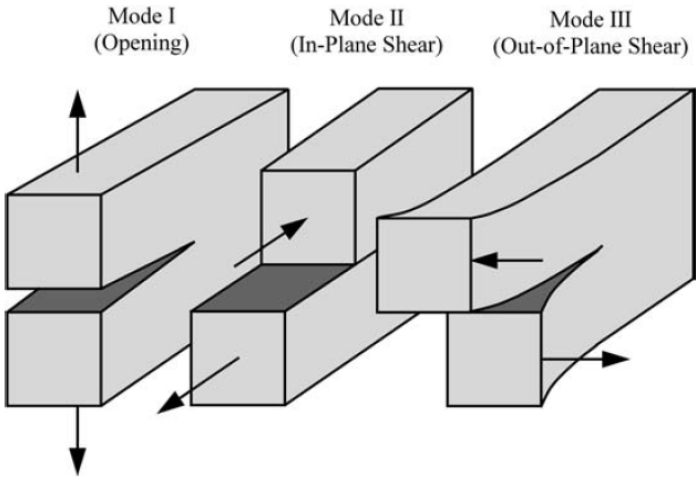

FIGURE 3.2 – The three loading modes that can be applied to a crack (ANDERSON, 2005)

The axial and bending load will mainly influence Mode I and the torque will affect Mode II. In this research Mode III is not considered, because the load on the shaft will not cause out-of-plane shear. Because of the combination of the loading types, multiple SIF's need to be considered for the different modes, SIF for Mode I (K_I) and for Mode II (K_{II}). The SIF will have multiple components and an equivalent SIF (K_{eq}) needs to be used for crack propagation calculations. Different methods for defining the K_{eq} are studied. According to Sajith et al. (SAJITH *et al.*, 2018), the prediction of fatigue life using Irwin's model aligns more closely with the experimental fatigue life. This model is expressed as:

$$K_{eq} = \sqrt{K_I^2 + K_{II}^2} \tag{3.8}$$

This K_{eq} can be substituted into Equation 3.7 to account for the mixed-mode loading.

$$\Delta a_B = \sum_{j=1}^{N_B} C_0 \left[\frac{\Delta K_{eq\,j}}{(1 - R_j)^{1-\gamma}} \right]^m \tag{3.9}$$

3.4 Crack propagation direction

Crack propagation will take place once a crack has been initiated. This crack initiation can be found using for example vibration analysis and rotor dynamics (stiffness reduction). Subsequently, the crack growth can be determined for each cycle, as discussed in previous subsections. This crack growth will be under mixed-mode loading, which is not a problem for calculating the crack growth rate. However, it might cause a problem with the crack propagation direction. The torque on the shaft will cause the crack to propagate under an angle. And because of the changing load combination, this angle might vary as well.

In Section 2.7 it is discussed that different crack propagation simulation programs are available. The main issue with those simulation programs, is that they use one certain cyclic loading. Which is not the case in this research.

For modeling the crack propagation in this research some assumptions are made. The crack angle is found using Abaqus. As discussed in Section 3.1, the criterion used in this research is the MERR criterion. The crack will propagate in the direction that maximizes the energy release rate. Furthermore, Anderson states that the maximum energy release rate will be highest when the kink angle is in the same direction as the main fracture (ANDERSON, 2005). Therefore, it is assumed that the angle under which the crack propagates will remain the same.

3.5 Degradation paths

Now that it is known how the crack will propagate, it is time to use this information for RUL predictions and maintenance purposes. The crack propagation can be simulated per flight cycle. The crack propagation per flight cycle can be combined to create the so called degradation paths. These paths can be plotted in graphs, like Figure 2.5, and useful information can be subtracted.

3.6 Failure threshold value

An important part of the degradation path models is the failure threshold value. This threshold value can be seen as the failure condition, at what point the part or system will fail. In most cases this is a predefined threshold that defines failure. However, real-world scenarios may pose a challenge for designers as they may not have access to precise information regarding the critical degradation level and associated uncertainties. Usynin et al. describe this in their research, called “Uncertain failure thresholds in cumulative damage models” (USYNIN *et al.*, 2008).

In this research this uncertainty is not taken into account and the failure threshold value is predefined. As can be seen in Figure 2.6, the fracture happens when ΔK reaches the fracture toughness (K_{Ic}). The fracture toughness of two materials is given in Table 4.1. And the ΔK value that is relevant in this case, is the $\overline{\Delta K}$ that is calculated using Equation 3.3.

3.7 RUL estimation

Based on the degradation paths and failure threshold values discussed in last subsections, the RUL can be estimated. Because of variability in the loading, a variation in the degradation paths is present. To account for this variation, a Probability Density Function (PDF) of the RUL is created. This can be done using the Monte Carlo simulation method. With this Monte Carlo method, results can be computed using iterative random sampling, followed by statistical analysis. This simulation method is closely related to random experiments, where the exact outcome is not known in advance (RAYCHAUDHURI, 2008).

Using this method, many crack growth simulations are performed. Every simulation gives the number of flight cycles at which the shaft will probably fail. With this data a PDF of the moment of failure can be constructed and the RUL can be estimated.

4 Crack propagation in the EC225 main rotor shaft

Last chapter presented a framework for determining the RUL, using Abaqus and fracture mechanics. In this chapter, the first part of this framework is discussed. The model EC225 Helicopter is used for crack propagation calculations of the main rotor shaft, which is used for RUL estimations in Chapter 5. The crack propagation is calculated using Abaqus and Matlab. The procedure for these simulations and calculations is outlined in the flowchart in Figure 4.1.

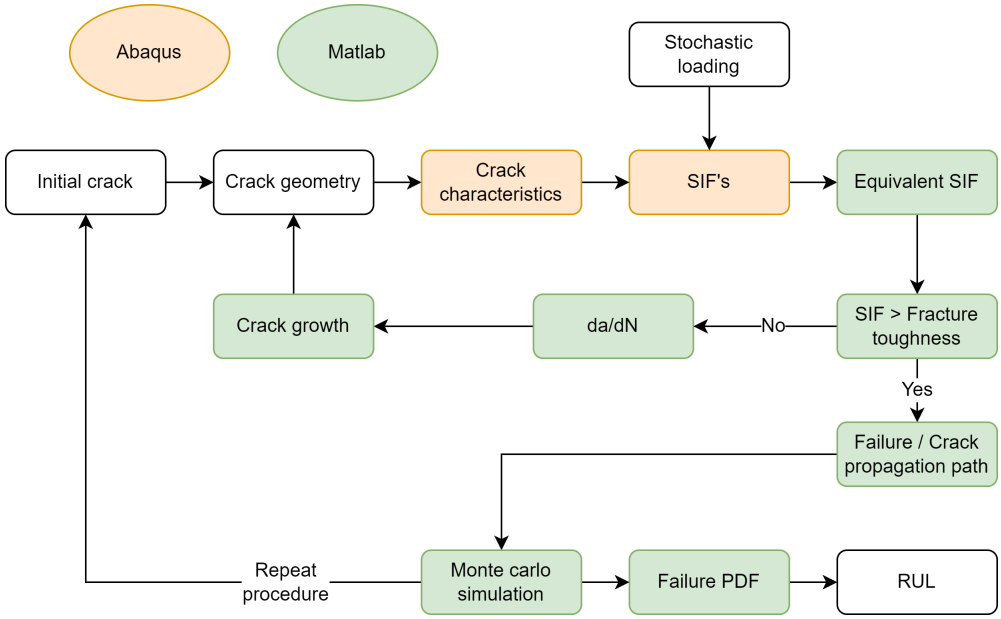

FIGURE 4.1 – Flowchart for determining the RUL based on crack propagation

The procedure starts with an initial crack with a certain crack geometry. This is used for characterization and obtaining the SIF's using Abaqus. These SIF's are then used in Matlab to determine the K_{eq}. It is checked if the K_{eq} reaches K_{Ic}. If not, the crack propagation is determined and a new crack geometry is considered, including new SIF's and a K_{eq}. This iterative process is repeated until the K_{eq} reaches K_{Ic}. When this happens, failure occurs and a crack propagation path is created until failure. Considering the Monte Carlo simulation method, this process is repeated multiple times. And multiple degradation paths are constructed. Based on this failure data, a failure PDF is obtained, which is used for RUL estimations. In this chapter the different parts of the flowchart are discussed by means of the EC225 main rotor shaft.

4.1 Main rotor shaft model

The Abaqus model of the main rotor shaft is created using the situation representation from Section 2.1. The in Abaqus created model contains the dimensions, material, and important constraints as will be discussed in Sections 4.1.1, 4.1.2 and 4.1.3.

In Abaqus three models for different steps in the process are created. (1) The shaft without a crack. This to find the stress intensity location and therewith the crack location. This will be discussed in Section 4.1.4. (2) The shaft with a 1 mm initial crack. By analysing this simulation, the crack propagation direction can be found, discussed in Section 4.3.2.1. (3) And the shaft with the initial crack and the crack propagation in a certain direction. Which is used for the final crack propagation analysis and establishing the degradation paths.

4.1.1 Shaft configuration and dimensions

As shown in Figure 2.2, sub-components are present around the main rotor shaft. If all sub-components are taken into account, a very complicated model will be created. Therefore, a simplified configuration is used to simulate the shaft in Abaqus. The shaft is connected rigidly with the MGB and supported by two bearing-like components. The shaft can move freely at the end of the axle, where the rotor is located. A schematic representation of the situation is given in Figure 4.2.

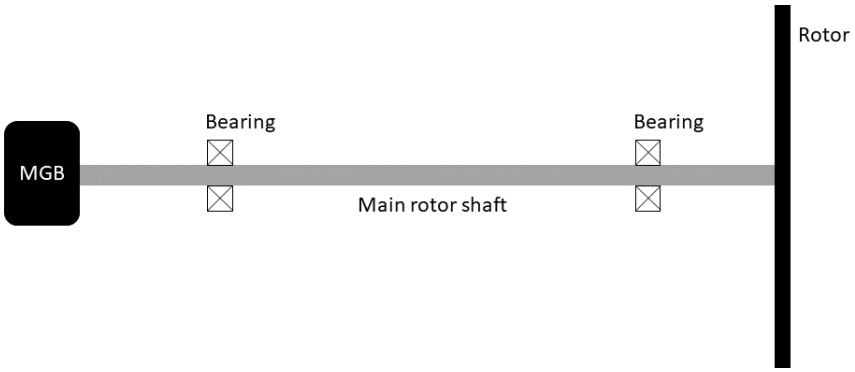

FIGURE 4.2 – Schematic representation of the main rotor shaft configuration

The main rotor shaft is described as a hollow cylinder. And the thickness of the shaft can be assumed to be 5.2 mm (AAIB, 2014). Unfortunately it was not possible to receive the exact dimensions for the length and the diameter. However, an estimation can be made, based on the main helicopter dimensions from Figure 4.3. It is assumed that the shaft has a length of 1 meter and a diameter of 120 mm.

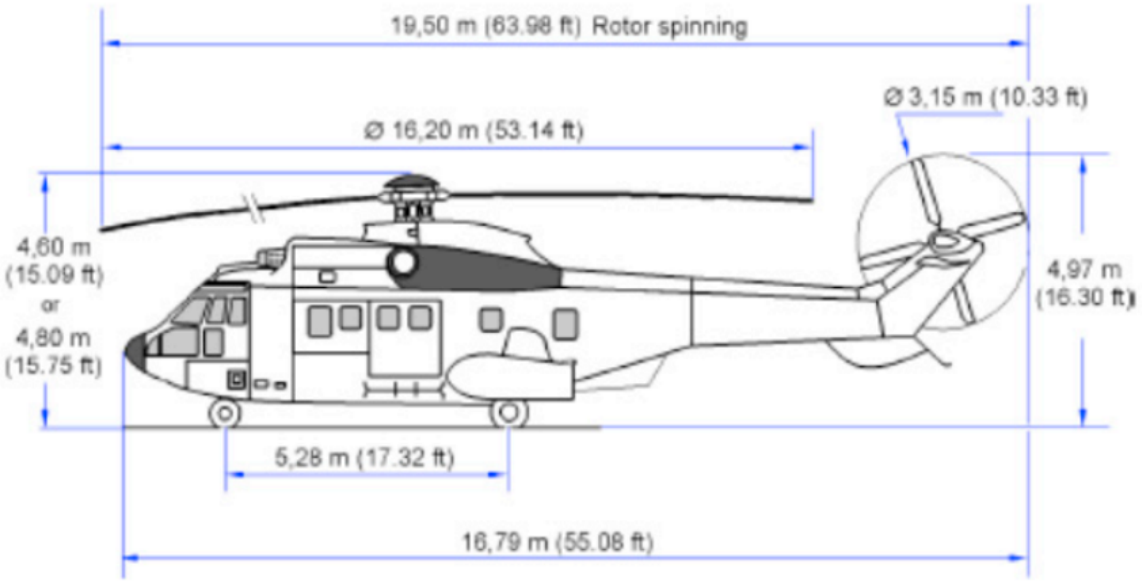

FIGURE 4.3 – EC225 helicopter dimensions (AIRBUS, 2015)

4.1.2 Material properties

Literature shows that the aerospace industry uses titanium as replacement for stainless steels like AISI 4340 (BOYER, 1994). The reason for this is the attractive properties like comparable strength, with weight reduction. It is stated that Eurocopter made the switch to the titanium Ti-10V-2Fe-3Al (Ti-10-2-3) for the front and rear rotor shaft as well as the blade-to-shaft attachment fitting, due to its exceptional tensile and fatigue strengths.

In this research the more general titanium Ti-6Al-4V (Ti-6-4) is used. All necessary properties and parameters are available for this material and the exact material properties are not of the utmost importance. The importance of this research lies in the framework and procedure. In Subsection 5.3.4 a comparison with an AISI 4340 stainless steel main rotor shaft will be made as well.

The properties of Ti-6-4 and AISI 4340 steel are based on the book of Dowling (DOWLING, 2013). The material constants for the Walker Equation, C_0, m and γ, are used for the crack propagation calculations. For AISI 4340 these parameters are available in the book of Downling. For Ti-6-4 this was not the case and the values are derived using available experimental data from the MMPDS handbook about Titanium alloys (FAA, 2013). The derivation is discussed in Appendix A. All properties are shown in Table 4.1.

TABLE 4.1 – Material properties of Titanium Ti-6Al-4V and AISI 4340 Steel

Property	**Symbol**	**Ti-6Al-4V**	**AISI 4340**	**Unit**
Elastic Modulus	E	117	207	[GPa]
Poisson's Ratio	ν	0.342	0.29	
Yield strength	σ_0	925	1255	[MPa]
Ultimate strength	σ_u	1000	1296	[MPa]
Fracture Toughness	K_{Ic}	66	70	[MPa$\sqrt{m}$]
Density	ρ	4.5	7.9	[g/cm^3]
Material constant (when R = 0)	C_0	1.602 x 10^{-8}	5.11 x 10^{-10}	$\left[\frac{\text{mm/cycle}}{(\text{MPa}\sqrt{\text{m}})^{\text{m}}}\right]$
Material constant	m	3.259	3.24	
Material constant	γ	0.709	0.420	

4.1.3 Abaqus model

The dimensions and material properties mentioned in sections 4.1.1 and 4.1.2 are used to model the main rotor shaft in Abaqus. The schematic representation in Figure 4.2 shows that the shaft consists of four connections: the MGB, two bearings and the connection with the rotors. These connections are modelled as boundary conditions in the Abaqus model. The modelled shaft is shown in Figure 4.4.

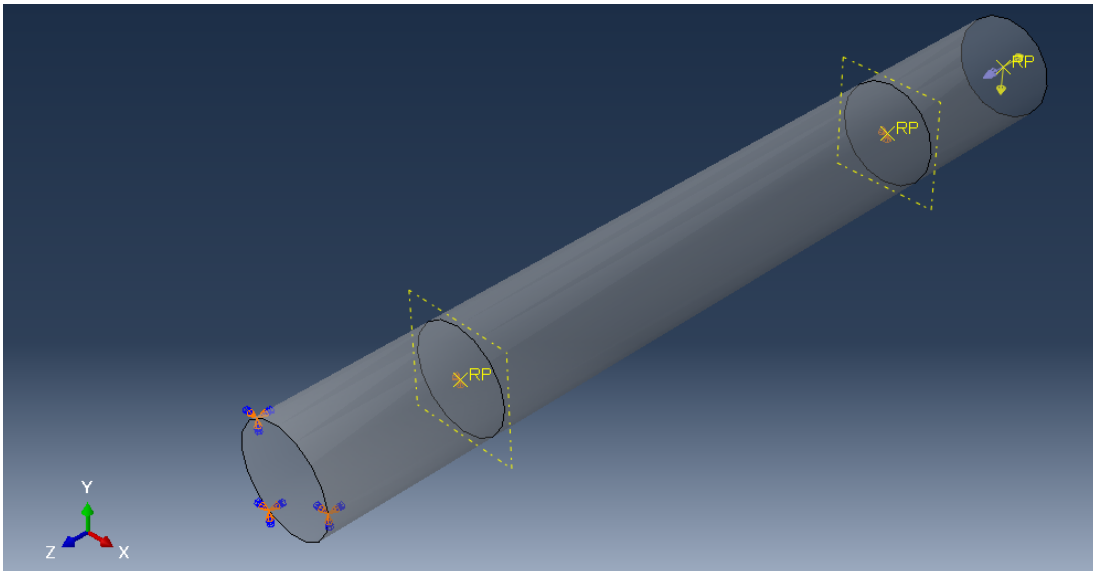

FIGURE 4.4 – In Abaqus modelled shaft, used for the analysis

The connection with the MGB is located at the bottom of the shaft in Figure 4.4. This shaft end is fully constraint, indicated with the orange/blue coordinate systems. The two bearings are located at the two intersections. These locations are constraint as a bearing, with no displacement in x and y direction. The top end is the place where the blades are located. This end is not constraint and is therefore free to move. Because this is the location of the blades, this position is chosen to be the location on which all forces act.

4.1.4 Crack location

The location of the crack is important for the analysis, as different locations have different stress levels. And different stress levels have different crack characteristics. It is assumed that the crack will initiate at the point where the stress level is highest. Two methods are used to find this location: Simple load diagrams and an Abaqus simulation.

The load diagrams are shown in Appendix B. These diagrams indicate the highest stress level to be located at the second bearing. The Abaqus simulation shows the same result. The modeled shaft is subjected to a combinations of axial, bending and torque loading. In Figure 4.5, the deformed shaft is shown. The stress concentration is clearly visible at the second bearing at the opposite side of the direction in which the bending takes place, the red areas. It is assumed that the crack will initiate at this stress concentration location.

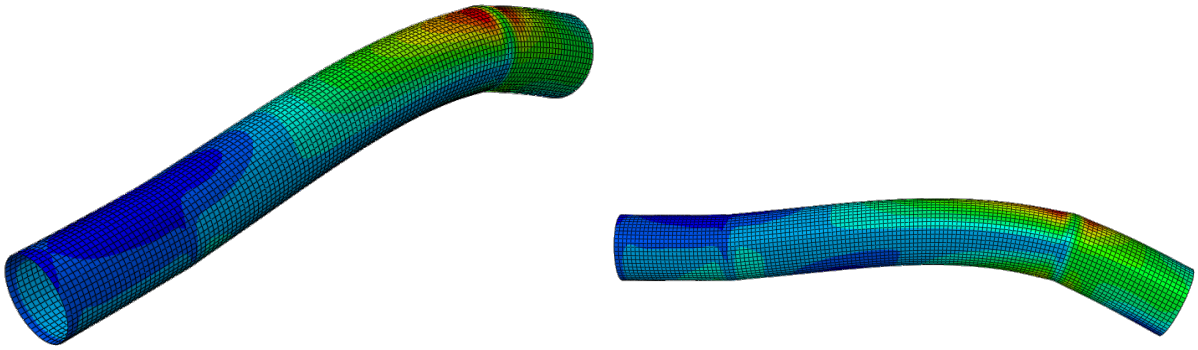

(a) (b)

FIGURE 4.5 – Visualisation of the deformed shaft (scaled), isometric (a) and side (b) view. With clearly visible stress concentration at red areas

4.2 Load input

An important element for the RUL estimations is the load to which the main rotor shaft is subjected. The assumptions and values for this load, loading sequence and how it is applied, are discussed in this subsection.

4.2.1 Loading assumptions

During operation the main rotor shaft is subjected to different loading types. These loading types are categorised into: (1) Axial Loading; (2) Bending; (3) Moment or torque. Some assumptions need to be made, to define the loading in this research and carry out the analysis:

- The axial loading is created by the lift of the helicopter itself
- Bending will mainly happen during flying and manoeuvre and is a result of for example wind, movement and environment
- The moment exerted on the shaft is mainly a consequence of the torque created by the MGB
- The loading is applied in a non-rotating configuration, as a fixed cylinder

Within fracture mechanics the amount of cycles between stress levels is important, not the time at a certain stress level. Therefore, in this research the analysis is done using only cycles between stress levels and not the time at a certain stress level. Every flight cycle is defined as one repetition, consisting of take-off, flying/hovering/manoeuvre and landing. More about this flight cycle is described in Section 4.2.3

4.2.2 Load specification

For constructing the model, the loads are specified as follows:

- The axial load is based on the weight of the helicopter, being the maximum gross weight of 11 000 kg (AIRBUS, 2015), which is assumed to be equal to an axial force of 110 000 N
- The bending load is assumed to be half the axial force, 55 000 N
- The moment load exerted on a helicopter main rotor shaft is given by Goodno and Gere (GOODNO; GERE, 2012) as 2.4 kN*m, this value is used in this research

These loading values are fixed values. However, in real life these values will vary, due to for example environmental influences or manoeuvres. Therefore, the input loads will be modeled as PDF's with certain distributions around the specified load. The variable input loads are also used to show how the model responds to stochastic inputs. These load distributions are defined in Section 4.2.4.

4.2.3 Loading sequence

In Section 4.2.1 assumptions are made on the loading of the shaft. The load consists of the three types. These three types of loading are present during operation and will cause the crack to propagate. This propagation will happen during every loading cycle within every flight cycle. Therefore, it is important to know what loading cycles are present during every flight.

In 1984 a standard was created for loading sequences related to helicopter rotors (EDWARDS; DARTS, 1984). This standard is used as a convenient tool for obtaining fatigue data for rotors subjected to realistic loading conditions. In this research the focus is on the rotor shaft instead of the rotors. However, this standard can be used as a basis for defining the loading sequence during one flight. There are two standards described, Helix and Felix. For this research, the Felix loading standard is used for determination of the loading sequence, as this standard is for fixed or semi-rigid rotors, and is therefore closest to the researched situation.

Using a modified version of this Felix standard, Felix/28, a loading sequence is constructed for this research. The loading sequence is shown in the graph of Figure 4.6. More information on the construction of this loading sequence can be found in Appendix C.

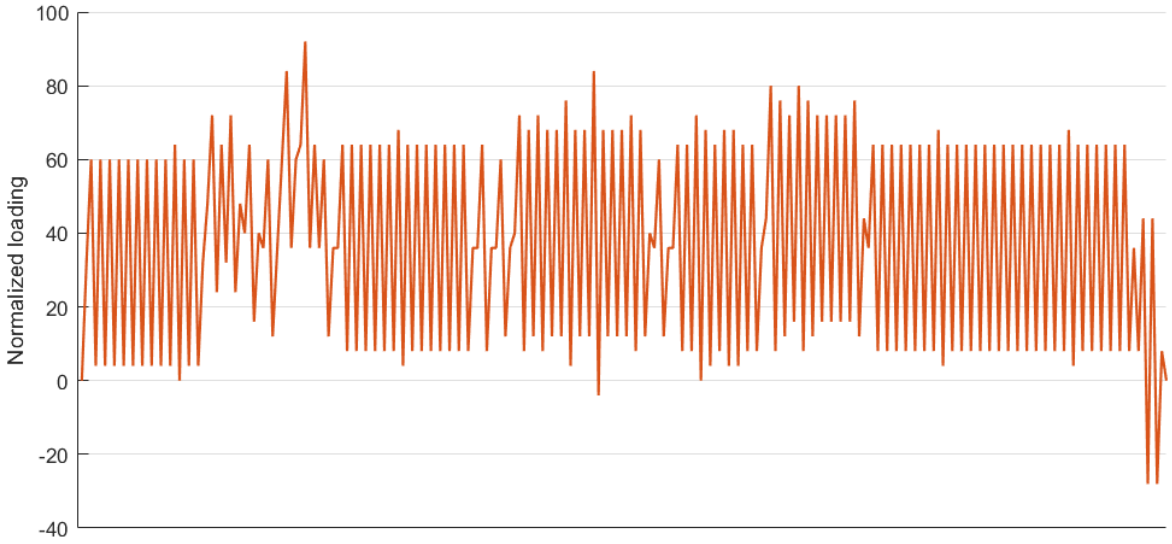

FIGURE 4.6 – Loading sequence based on the Felix/28 standard (EDWARDS; DARTS, 1984)

This loading sequence indicates the load on a scale up to 100, equal to the percentage of the load specified in Section 4.2.2. The loading sequence and its values are used in the deterministic model for crack propagation. Every single cycle in this loading sequence has its contribution to the crack propagation.

4.2.4 Probability Density Function (PDF) of loading inputs

Section 4.2.2 already mentioned that the load input is modelled as a PDF, to account for variance in loading. These variable loads show how the model responds to a stochastic input. In this research, the PDF for the loading is defined as shown in Figures 4.7 a-c. This PDF is used to take load values randomly for every manoeuvre in the load sequence, which is then scaled to fit the loading sequence values.

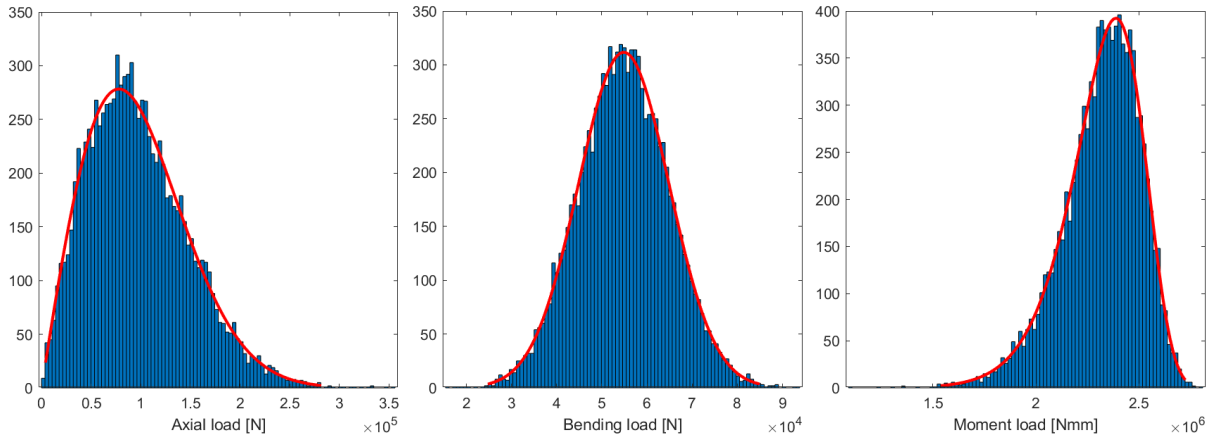

(a) (b) (c)

FIGURE 4.7 – PDF of the different load inputs: (a) Weibull distribution for axial loading, (b) and (c) Normal distribution for bending load and moment load respectively.

The distributions shown in Figure 4.7 are a representation of 10000 random chosen values following a predefined distribution. For axial and moment loading a Weibull distribution is chosen and for the bending load a normal distribution. In this research the loading data and distribution is assumed and predefined. However, with available real-life data about the loading, real distributions of real loading can be implemented easily for real-life analysis.

4.3 Relation between SIF, load and crack length

As discussed, different loads and load combinations will act on the shaft. These different loading inputs will result in different outputs from Abaqus and Matlab. Besides, the crack geometry will change constantly because of the crack propagation, causing different outputs from Abaqus as well. In short the SIF can be seen as a function of load and crack geometry and Abaqus is used to define this relation. In upcoming subsections this relation is elaborated further.

4.3.1 Load change and SIF

The SIF need to be determined for every crack length and for every loading combination. At first, this seems like a very time consuming and inefficient way, but a more optimal solution is found. Because the stress analysis is based on linear elastic mechanics, it can be stated that the SIF has a linear relation with the load. Therefore, it is possible to derive one baseline relation between the SIF and a load. Subsequently, a new SIF can be obtained for the load of interest, by multiplying the baseline SIF with the ratio between

the load of interest and the baseline load (ZHAO *et al.*, 2015).

One of the problems in this research is the combination of loads, multiple different loads are acting on the shaft at the same time. In the Abaqus model it is found that in this case superposition of the SIF for the different loads is valid. This means that it is not necessary to run the finite element model for every possible loading combination, only for a certain crack length. This principle is explained in more detail in Appendix D. In this appendix a mathematical explanation is given to clarify the relation between the SIF and load changes.

4.3.2 Geometry change and SIF

Now the linear relation between the SIF and the load is known, the relation between the geometry and the SIF needs to be determined. No similar linear relation is found that defines the SIF for geometry change. Therefore, the Abaqus model is used to determine the SIF at the baseline load for every crack size. Assumptions are made regarding the crack propagation and the geometry change, discussed in the subsections below.

4.3.2.1 Crack propagation direction

In Section 3.4 assumptions are made about the crack propagation direction. The crack will propagate under an angle and will keep propagating under that angle. With the use of Abaqus, the MERR directions are found for different loading combinations at the initial crack length of 1 mm. For both the crack ends these MERR directions are determined. For determining the MERR directions, the crack tip and crack front is defined in Abaqus. The crack propagation angle is measured with respect to the crack plane, in counterclockwise direction (SIMULIA, 2006) and given in Table 4.2.

TABLE 4.2 – Loading combinations and propagation angle for both crack ends (MERR direction)

Axial [N]	**Bending [N]**	**Moment [Nmm]**	**Angle C1 [Deg]**	**Angle C2 [Deg]**
110000	0	0	0	0
0	55000	0	0	0
0	0	2400000	75.78	75.78
110000	55000	2400000	9.65	9.50
11000	5500	240000	9.65	9.50
36667	18333	800000	9.65	9.50
110000	55000	800000	3.74	3.49
110000	18333	2400000	18.90	18.79
36667	55000	2400000	11.16	11.02
80000	40000	2000000	10.84	10.9
80000	40000	150000	8.532	8.388

In the table it can be seen that the angle of crack propagation is mainly caused by the moment acting on the shaft. When the load is equal to the in Section 4.2.2 specified

loading conditions, a crack angle of around 9.58 degrees is found. This angle remains the same for loading conditions with the same loading ratio between axial, bending and moment loading. For both crack ends, the angles have negligible differences and can be assumed similar. When the ratio of loading combinations differs, the angle differs as well. With relatively higher moment loading, the angle will increase. And with relatively higher axial and/or bending load, the angle will decrease.

As shown, variability is possible, but not taken into account in this research. In this research it is assumed that the loading will be around the same ratio as the in Section 4.2.2 specified loads, and will therefore remain around 9.58 degrees. This angle will also be maintained during crack propagation.

4.3.2.2 Propagation behaviour

The crack in the shaft has two crack ends, both of which will propagate. It is assumed that both crack ends will propagate the same amount and in the same way during operation. If one crack side propagates more, the SIF increases at the other side, which in turn causes more propagation at this side. The crack propagation can therefore be considered to be in equilibrium.

The crack propagation can be simulated and analysed using XFEM in Abaqus as well. XFEM is used to visualise the crack propagation and validate the assumptions and results from Subsection 4.3.2.1. In the XFEM simulation, a loading combination of 100 times the in Section 4.2.2 specified loads is used, which is only used for simulating the crack propagation. The same ratio of loads is maintained: Axial = 1.1e7 N, Bending = 5.5e6 N and Moment = 2.4e8 Nmm. The result of the Abaqus crack propagation simulation is shown in Figure 4.8.

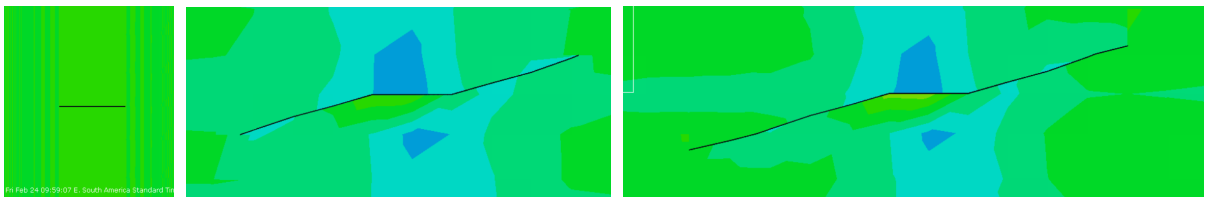

(a) (b) (c)

FIGURE 4.8 – Abaqus crack propagation simulation using XFEM, for visualisation of propagation behaviour. Propagation: (a) Initial crack of 1 mm, (b) intermediate crack propagation and (c) final stage crack propagation

It can be seen that the crack will propagate under an angle and will stay under this angle. It is also clearly visible that the crack propagation will be equal on both sides of the crack. This proves that it is likely that the assumptions made earlier are correct.

4.3.3 Abaqus output

Abaqus is used to find the SIF's at a certain load and crack geometry, this output can be described as: the SIF's at the baseline loading for axial, bending and moment load, for different crack lengths.

These SIF's are obtained using a modelled crack in Abaqus. As described in Section 4.1, three models are created. The first one, without a crack, is used to find the crack initiation location. The second one is the shaft with a 1 mm horizontal crack. From this model, the SIF's at 1 mm and the crack propagation direction is found. This crack propagation direction is used in the third model, in which the crack propagation under an angle of 9.58 degrees is modeled for different crack lengths. This model is used to obtain the SIF's at different crack lengths. The last two models are shown in Figure 4.9. Both models are loaded under the in Section 4.2.2 specified loading conditions.

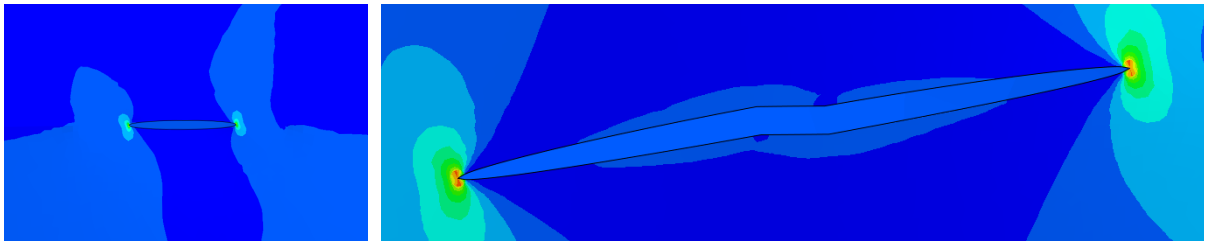

(a) (b)

FIGURE 4.9 – Abaqus simulation results of (a) the initial crack of 1 mm and (b) a crack of 10 mm (1 mm initial crack and 4.5 mm on both sides) under an angle of 9.58 degrees

The Abaqus output that useful for this research are the SIF's. These SIF's for a titanium shaft are given in Table E.1 in Appendix E. In this table the SIF for modes I and II are shown, for both crack sides, for every loading type and at a range of crack lengths.

These SIF's at the baseline loading for the different crack lengths can be seen as the basis for all calculations, the deterministic part. The right SIF for a certain scenario (loading combination and crack length) can be determined using the earlier described relation and the SIF at baseline. And the crack growth rate can be determined with the use of the right SIF's.

4.3.4 SIF as function of load and crack length

Now that for every crack length and load type, the SIF's for mode I and II for both sides of the crack and at the baseline loading has been obtained, it can be used for further calculations. These baseline SIF's can be scaled to many different loads, creating graphs described as SIF as function of load and crack length. The graphs for axial loading are

shown in Figure 4.10. In these graphs the SIF is given for both modes and both sides of the crack. The same relation is created for both bending and moment loading.

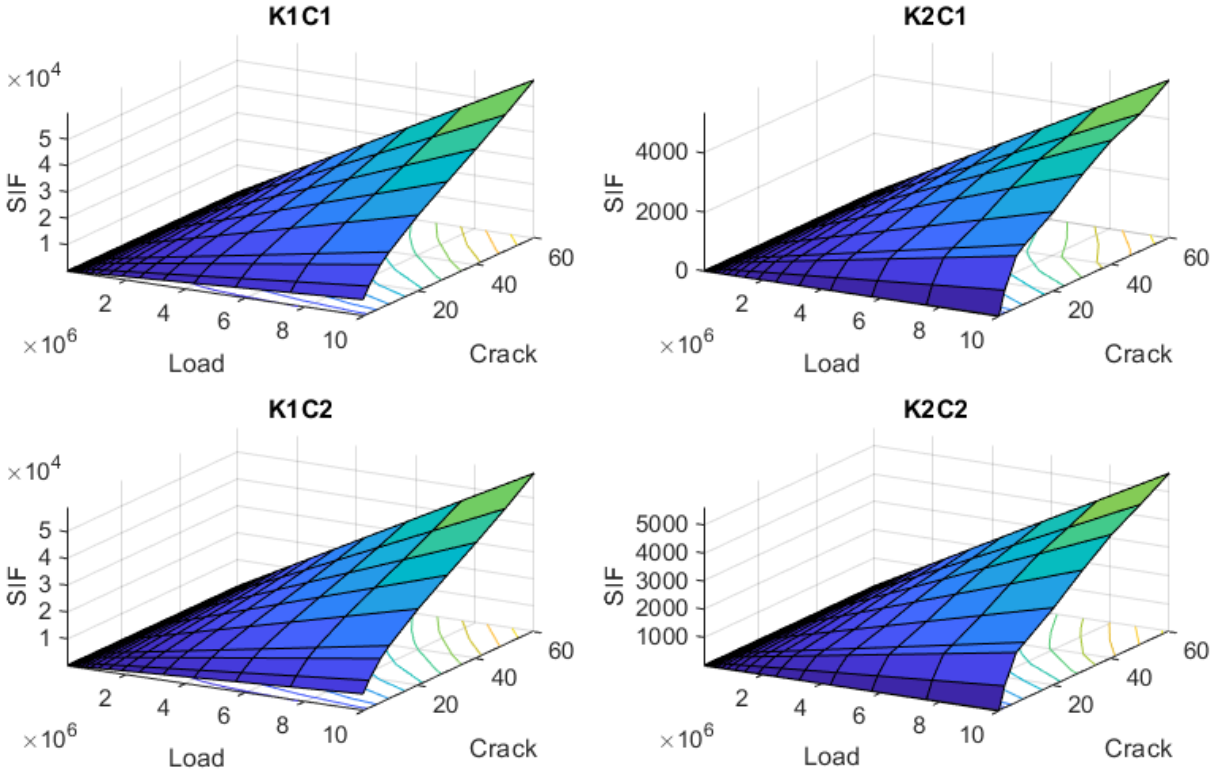

FIGURE 4.10 – SIF $[MPa/\sqrt{mm}]$ as function of load $[N]$ and crack size $[mm]$ for axial loading. For the SIF mode I or II (K1 and K2) and both crack side (C1 and C2)

4.4 Crack propagation and degradation paths

As described above, the crack can be characterized for the different scenarios and the crack propagation can be analysed. As explained in Section 3.2, this crack propagation can be calculated using the Paris equation or a modification on it. For every individual flight cycle the crack propagation can be calculated using Equation 3.7. In which the ΔK is the stress intensity range. This stress intensity range can be computed with the known SIF's. However, the values cannot be taken directly from the graphs in Figure 4.10. As discussed in section 4.3.1, superposition needs to be used for determining the SIF for a combination of different loads. Then the K_{eq} for both sides of the crack can be calculated and used in Equation 3.9.

During one flight cycle, many different smaller loading cycles are present, as shown in Figure 4.6. These smaller loading cycles will contribute to the crack propagation and are therefore taken into account during crack propagation calculations. Using the change in SIF's and Equation 3.9, the crack propagation during one flight is calculated.

This sequence is repeated for the next flights, with different load inputs and new crack characteristics. Until the crack reaches its threshold value and failure will happen. This sequence of crack propagation during the flights can be described as the degradation path. The degradation path of a shaft from crack initiation of 1 mm to failure is shown in Figure 4.11 a, the crack size is plotted against the number of flight cycles. However, because of the variability in the loading and therewith crack propagation, different degradation paths are possible. The same model can be run multiple times to see the variability in the results, shown in Figure 4.11 b.

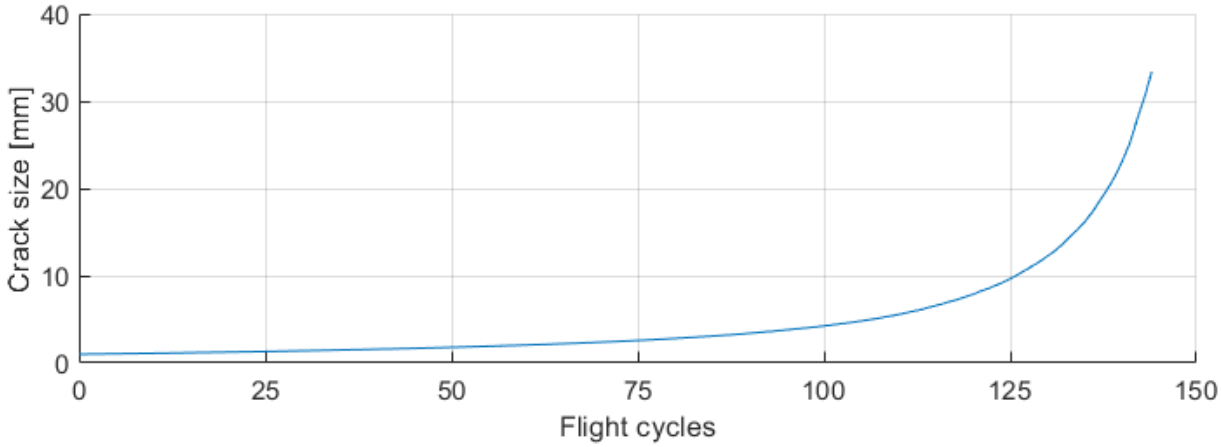

(a)

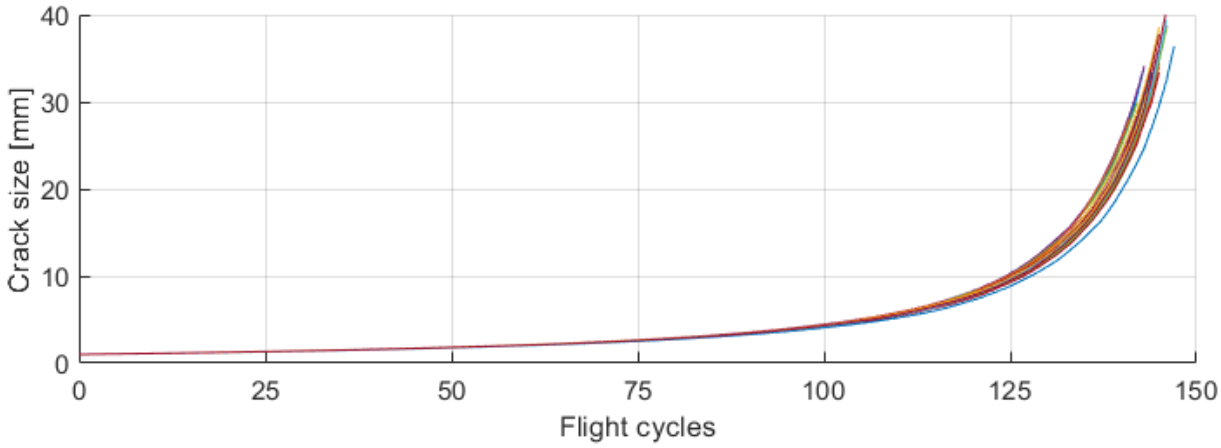

(b)

FIGURE 4.11 – The degradation path of one shaft (a) and multiple shafts (b) from crack initiation to failure. In which the crack size is plotted against the number of flight cycles.

The degradation paths from Figure 4.11 have a clear exponentially distribution. It shows the deteriorating and the increase in crack growth rate when the crack size increases. In the next chapter these degradation paths are used in the context of RUL and maintenance management.

5 Maintenance improvement

The degradation paths shown in Figure 4.11, are the number of flight cycles until the shaft will fail, in other words the time to failure. Knowledge about the time to failure can be useful for maintenance management. Decisions can be made based on this time to failure and maintenance can be improved.

When taking the average of multiple degradation paths, the Mean Time To Failure (MTTF) can be obtained. This MTTF is a quantity that is often used for system reliability. Another quantity that can be used for system reliability, is the Mean Time Between Failures (MTBF). Tinga (TINGA, 2013) described the difference between MTTF and MTBF as the repair period after failure. MTBF includes the Mean Time To Repair (MTTR) and MTTF not. In this research the RUL is estimated from a point of initial cracking of for example 1 mm, until the shaft will fail. In this estimation the MTTR is not taken into account, so only the MTTF is considered in this research.

In next subsection, it is discussed how the MTTF and RUL are obtained statistically. Section 5.2 discusses how RUL estimations can influence the maintenance planning. The variability of the model input and its influence on the RUL estimation is discussed in Section 5.3. And this chapter ends with putting RUL into the bigger picture of RCM, discussed in Section 5.4.

5.1 MTTF and RUL

The variation in the degradation paths and therewith RUL can be expressed as a PDF. And as described in Section 3.7, this can be done using the Monte Carlo simulation method. In total 2000 iterations are carried out, so 2000 degradation paths are created. In Appendix F it is explained why a number of 2000 iterations is chosen. These 2000 degradation paths are shown in Figure 5.1a. From this Monte Carlo simulation, a histogram can be created about the number of flights until the shaft fails. In Figure 5.1b this histogram is shown, with on top a distribution of this time to failure data. The distribution chosen to be most suitable is the Weibull distribution. The Weibull distribution is frequently used in reliability applications for aircraft systems, like for example fatigue life or crack growth rate scatter (OLIVEIRA, 2018).

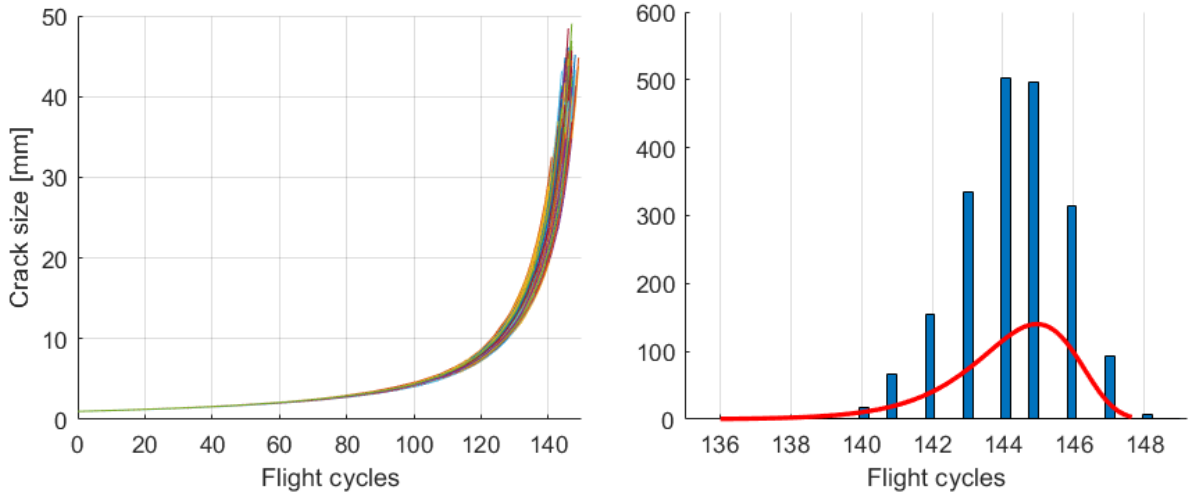

(a) (b)

FIGURE 5.1 – (a) Monte Carlo simulation of degradation paths and (b) histogram on time to failure data

In Figure 5.1b, it can be seen that most of the degradation paths end at 144-145 flight cycles. This indicates that it is most likely that the shaft will fail around these numbers of flight cycles. Using the Weibull distribution it is possible to predict the so called MTTF, or in this research the RUL. The equation for calculating the RUL is given as (PRENSCIA, 2001):

$$RUL = \eta * \Gamma\left(\frac{1}{\beta} + 1\right) \tag{5.1}$$

In which η is the scale parameter and β the shape parameter of the Weibull distribution. The Γ is the gamma function, defined as:

$$\Gamma\left(\frac{1}{\beta} + 1\right) = \int_0^\infty e^{-x} x^{\left(\frac{1}{\beta}+1\right)-1} dx \tag{5.2}$$

For determining the RUL, the scale and shape parameter for the Weibull distribution need to be defined. This is done by fitting the probability distribution in MATLAB, shown in Figure 5.2.

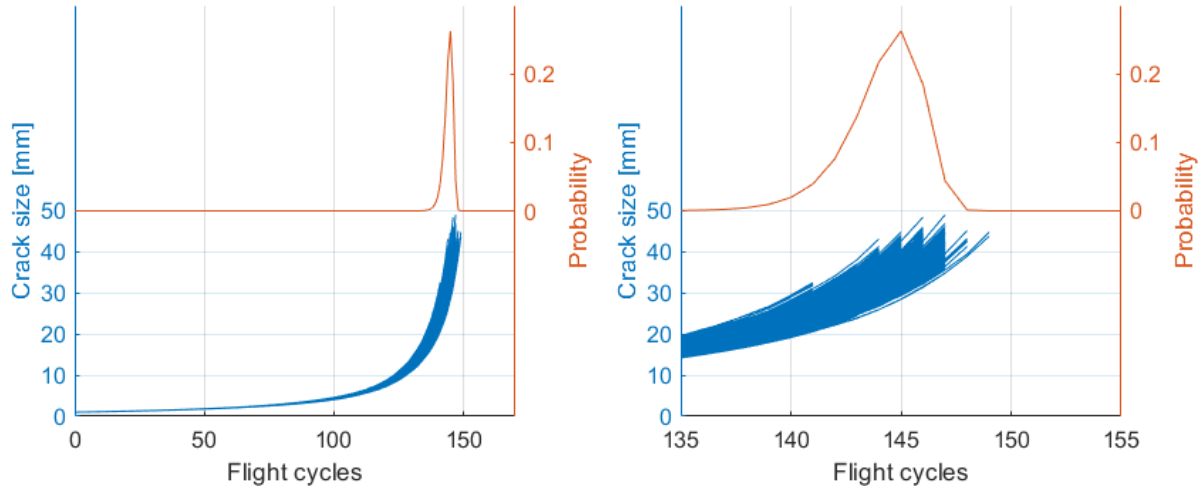

(a) (b)

FIGURE 5.2 – Degradation paths and corresponding Weibull distribution, (a) normal view, (b) zoomed in view

Using the parameters of the Weibull distribution and Equation 5.1, the RUL is calculated to be 144.18 flight cycles.

5.2 Maintenance planning and RUL

Now that the RUL can be determined, it can be used for maintenance purposes. First of all, to determine the inspection interval, but also certain decisions for certain scenarios can be anticipated.

5.2.1 Inspection interval

Because of uncertainties in the actual stress, initial crack size and crack growth rate, safety factors are needed. This safety factor can be implemented into the system as periodic inspections.

It is important that the safety factor ensures that cracks will not grow to failure between inspections. It is possible that an initial crack is missed during the first inspection, and a second inspection is necessary. In aviation a safety factor of 1.5 is normally applied to the loads present on a aircraft (ZIPAY *et al.*, 2016). However, it is better to choose a safety factor of around 2.5 for this crack propagation problem. The inspection interval (N_I) can be determined using the following equation:

$$N_I = \frac{RUL}{X} = \frac{144.18}{2.5} = 57.67 \text{ flight cycles} \tag{5.3}$$

This inspection interval is shown in Figure 5.3 as the vertical black lines. Because of the safety factor of 2.5, two inspections are carried out before the shaft will fail. This to ensure that the crack will not grow to failure between inspection.

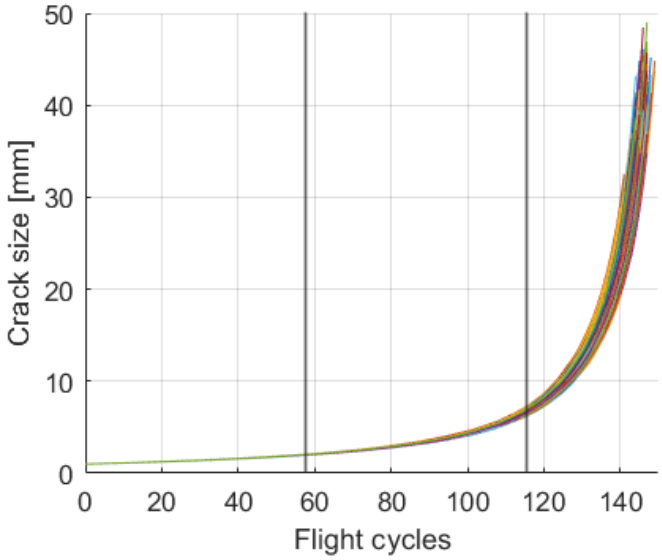

FIGURE 5.3 – Degradation paths with periodic inspection intervals, indicated by the vertical black lines

This inspection interval does not need to be considered or considered differently, when the crack propagation is monitored using a system like the HUMS.

5.2.2 Maintenance scenario's

During inspection a crack is found or no crack is found. When there is no crack present, or the crack is smaller than the initial crack size, nothing will happen. The model is ran as before and the RUL will stay the same. The other situation is that a crack is found with a certain crack length. In this situation the model can be ran with a different initial crack size and a new RUL can be determined.

In case a crack with a length of 4 mm has been found, new simulations are carried out to calculate the RUL from this new crack length. The results of this new simulation are shown in Figure 5.4 next to the old results. The RUL is determined to be 47.27 flight cycles. Because of the larger initial crack size the probability of this RUL is higher, with less variance and with less uncertainty.

In this case the decision can be made to plan the maintenance within this RUL of 47.27 flight cycles, to replace or repair the shaft. However, it is also possible to extend the RUL by reducing the load applied on the shaft and therewith the crack growth rate. This allows the amount of flights until the point maintenance is required to increase. In this case the maintenance can be postponed to a more convenient moment.

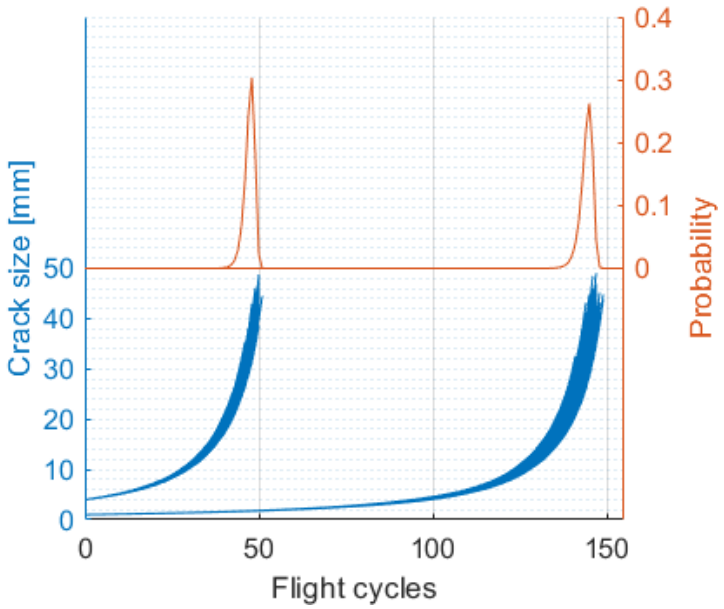

FIGURE 5.4 – New simulation after crack of 4 mm was found during inspection, degradation paths on the left

The same holds, a crack with length of 4 mm is present. But this time all three loading types are reduced by 5%. The results are shown in Figure 5.5, and the difference is clearly visible. By reducing the load, the RUL increases from 47.27 to 55.85 flight cycles.

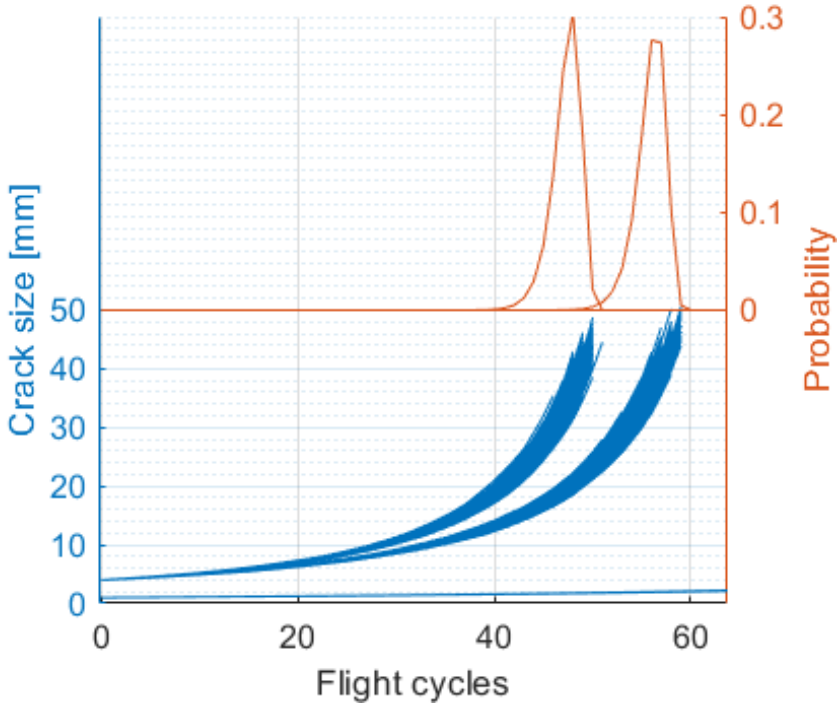

FIGURE 5.5 – New simulation after crack of 4 mm was found during inspection, with 5% reduction of the total load

5.3 Variability influence

The model is constructed and RUL estimations are obtained. Variables can and will influence the RUL estimations, as can be seen in Section 5.2.2. In this subsection, the effect of different loading amplitudes, loading input distributions, loading sequences and shaft material on the RUL estimation is shown.

In this research the input is simulated, the loading and loading sequence are defined and assumed. However, when real life data is available, this can be implemented easily and RUL estimations can be obtained. With knowledge about the effect of variability, maintenance management can be improved and well-informed decisions can be made. More about this is discussed in Section 5.4.

5.3.1 Loading amplitude variability

In Figure 5.5 the change in loading amplitude has already been discussed shortly. In this subsection this variability is discussed more extensively. Multiple simulations are carried out for different loading amplitudes and the RUL is estimated. In total nine different loading amplitudes are simulated, indicated with percentages of the in Section 4.2.2 specified loads: 80%, 90%, 95%, 100%, 105%, 110%, 120% and 140%. For every loading amplitude degradation paths are simulated using the model and shown in Figure 5.6.

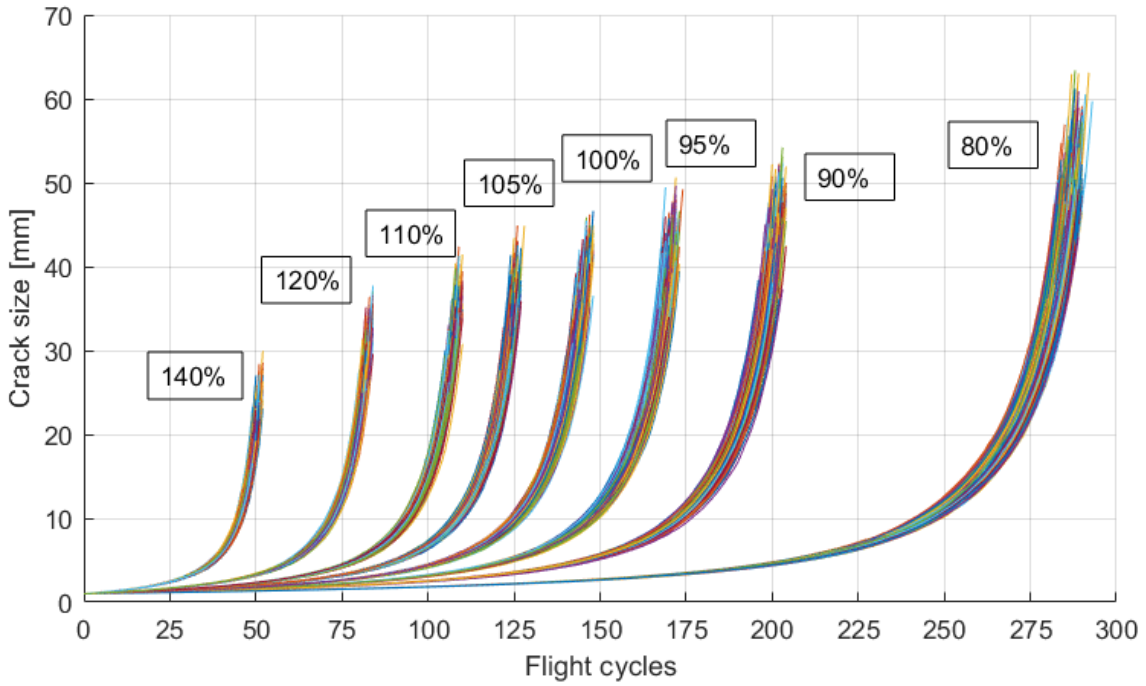

FIGURE 5.6 – Degradation paths of different loading amplitudes (in percentage of the in Section 4.2.2 specified load), indicated in the graph

What can be seen in the figure is that the flight cycles until failure increases when the load decreases. Also the crack length increases with decreasing load. This can be explained by the lower stress present in the crack, as a result of the lower loading amplitude. The crack propagation is therefore lower and more flights can be carried out with larger crack size until the shaft fails. For the different loading amplitudes, the RUL's are estimated. These estimations are shown in Figure 5.7.

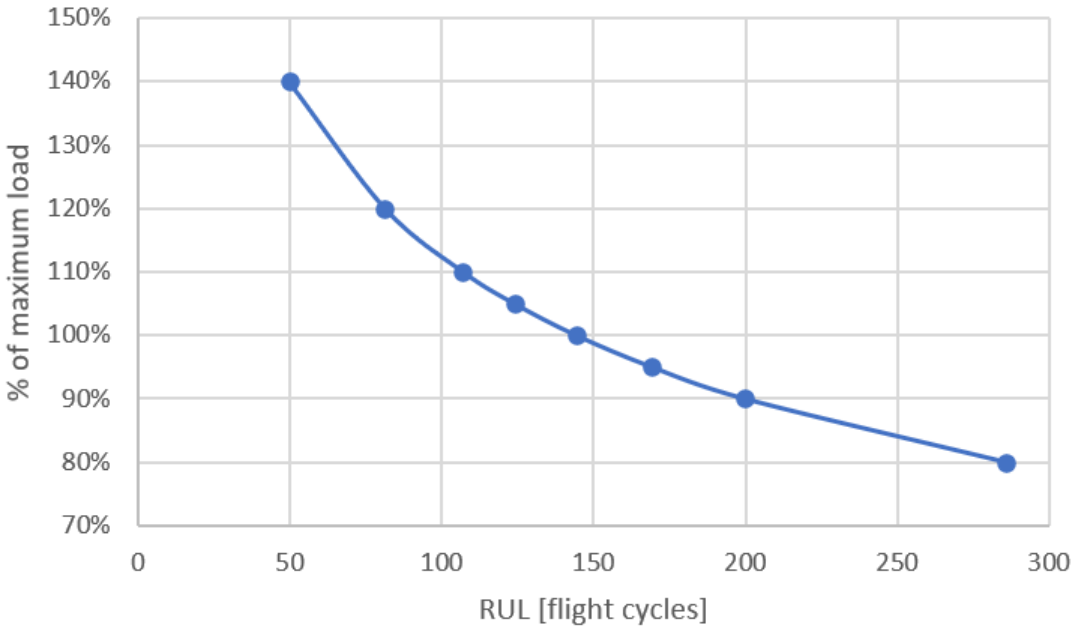

FIGURE 5.7 – Change in RUL for different loading amplitudes

It is clearly visible that the amplitude of the loading influences the RUL strongly. With increasing load, the RUL is decreasing and the other way around.

5.3.2 Loading input distribution variability

The load input consists of three PDF's, with a certain mean and variance or shape and scale parameter. The way the PDF's are constructed will have its influence on the results and RUL estimations. In this subsection changes in these distributions are discussed.

This research used one normal and two Weibull distributions for the load input, shown in Figure 4.7. In this example all three loading types are described by normal distributions. For which two scenarios are used: (1) Standard mean, with high variance and (2) Standard mean, with low variance. The results of the simulations are shown in Figure 5.8.

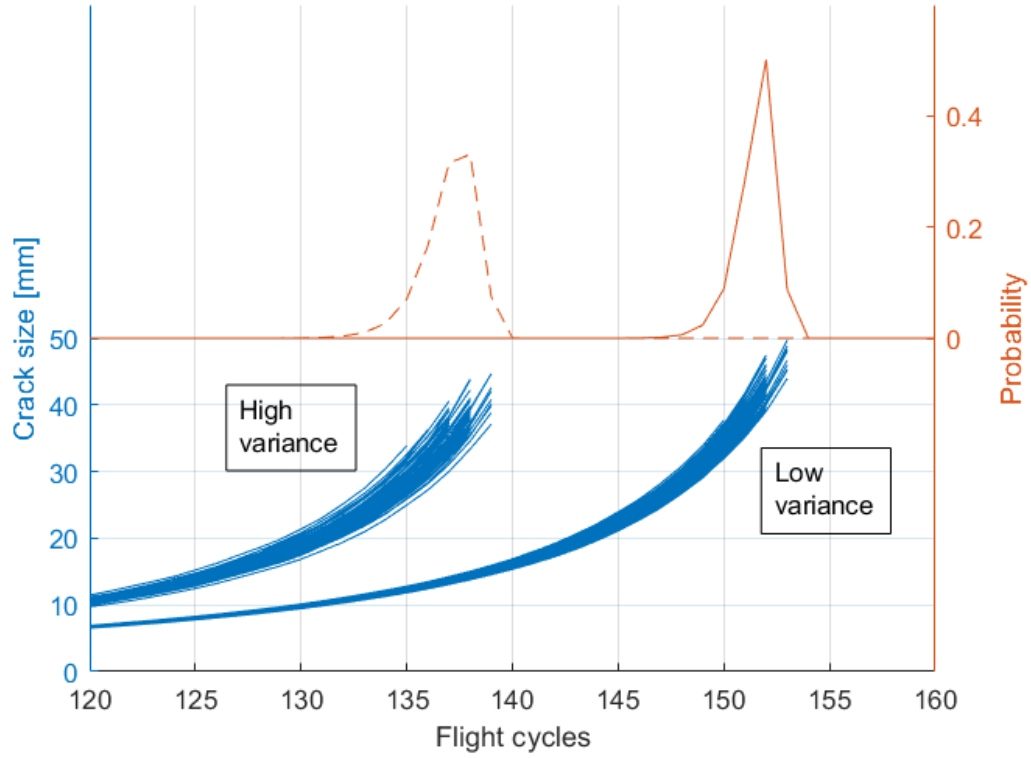

FIGURE 5.8 – Degradation paths of both high and low variance load input distributions. With in red the distribution of the RUL

In the figure it can be seen that when the variance of the input loading is high, the degradation paths are shorter and the distribution of the RUL has a higher variance. If the variance of the input loading is low, the crack in the shaft will propagate slower and the variance of the RUL is lower as well.

5.3.3 Loading sequence variability

The final part that defines the loading input in this research are the flight cycles and loading sequences. In this research only one loading sequence is used, discussed in Section 4.2.3. However, it is very likely that flights vary and one flight is more rough or more calm than the other. Three different types of flight cycles are simulated to show its influence on the RUL, a loading sequence for rough, normal and calm flights. The simulations are shown in Figure 5.9.

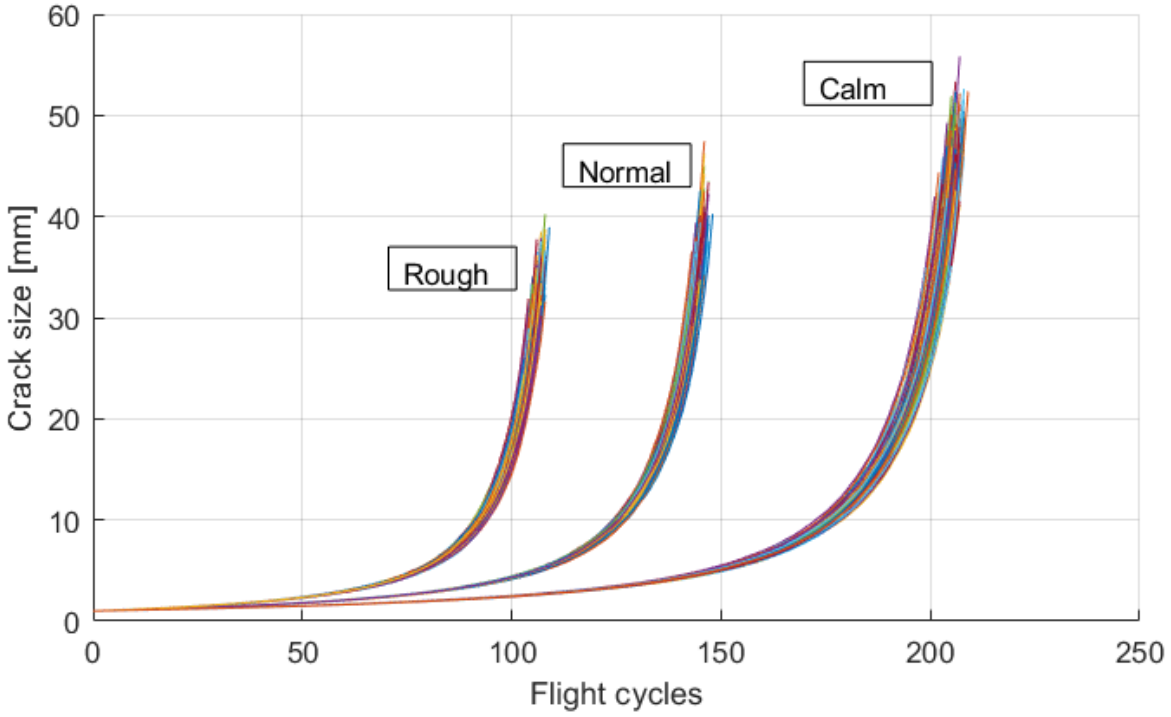

FIGURE 5.9 – Change in RUL for different loading sequence, indicating rough, normal and calm flight cycles

It can be seen and concluded that the calmer the flight, the higher the RUL is. Which is the same principle as can be seen in a change in loading amplitude. The calmer the flight, the lower the stress, the lower the crack propagation and the higher the RUL.

5.3.4 Material change

As already mentioned in Section 4.1.2, the aerospace industry replaced many stainless steel parts by titanium. This because of the attractive properties like comparable strength, with weight reduction. The model in this research can also be used to check the crack propagation and RUL for different materials, like the stainless steel. In this subsection the crack propagation and RUL estimation of Ti-6-4 is compared to AISI 4340 stainless steel. The circumstance are the same, but with different material properties and crack characteristics. The material properties are given in Table 4.1 and the crack characteristics, obtained by Abaqus, are given in Table E.2. For both materials, the degradation paths are simulated and the results are shown in Figure 5.10.

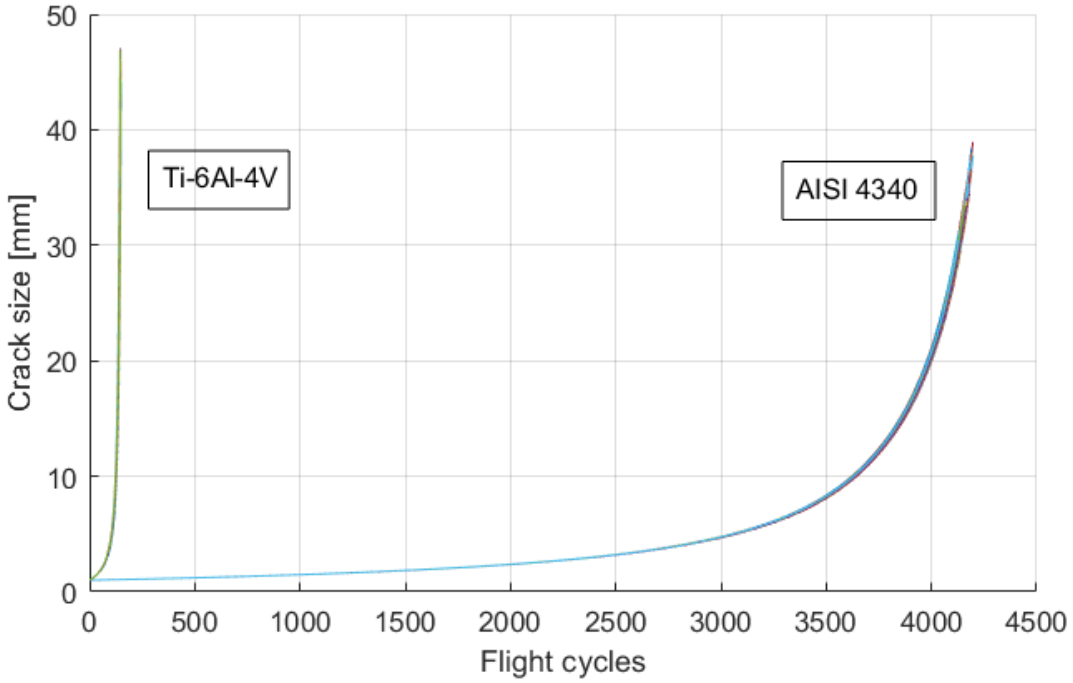

FIGURE 5.10 – Degradation paths for Ti-6Al-4V and AISI 4340

The difference between the two materials is clearly visible. The crack propagation for AISI 4340 is much slower compared to Ti-6-4, resulting in much more flight cycles to failure and therewith a much higher RUL. The SIF's from Tables E.1 and E.2 for both materials are similar, so the difference is mainly caused by the materials fatigue properties. This difference in material properties is visible in Table 4.1. The material constants for the Walker Equation, C_0, m and γ, are used for the crack propagation calculations and differ significantly. In this case it can be said that stainless steel would be more applicable. However, it is important to keep in mind that weight reduction is achieved by using titanium. Besides, the actual material is Ti-10-2-3, which has a higher strength and better fatigue properties compared to Ti-6-4 (BOYER, 1994).

5.4 RUL and RCM

In this research and for this application, the main rotor shaft, all three the criteria of RCM are important. Safety needs to be guaranteed at all time, shaft failure is unacceptable. Security must always be maintained and failure consequences must be reduced to the minimum. And eventually economics, all decisions need to be made taking minimum life-cycle costs into account.

In short, RCM should help to develop a technique to systematically assign the correct maintenance strategy to the system, where safety, security and economics are taken into

account. Eventually, decisions can be made for efficient maintenance planning, scheduled repair or replacement decisions, depending on multiple factors including the system or even a whole fleet. Also spare part management and stocking can be optimized.

In Sections 5.2 and 5.3 the RUL is estimated, inspection intervals are determined, maintenance scenarios are discussed and also the variability of the model is shown. All this data and information can be used for decision making for maintenance strategies. Decision with respect to safety, security and economics, in other words RCM.

A small example is most useful to explain the principle how RUL and RCM can be combined. A EC225 helicopter is part of a fleet with multiple helicopters. Vibration data of the main rotor shaft indicates a crack of 4 mm. Based on this initial crack of 4 mm, the RUL is estimated. For safety and security reasons maintenance needs to be carried out before a certain maximum number of flight cycles. However, because there is no space in the workshop, spare parts are not yet available or the helicopter is needed, from an economical perspective the helicopter needs to fly for a certain amount of flight cycles. Now a decision can be made on what is the best solution based on RCM, finding the most optimal solution regarding safety, security and economics. For example reaching a certain amount of flights in a safe and secure way, by lowering the overall load and changing the way the helicopter is used to a more calm flight. And therewith reaching all RCM criteria.

6 Conclusions

At the moment, maintenance to the main rotor shaft of the EC225 is carried out every 2,000 flying hours, when the MGB is overhauled. However, maintenance to the main rotor shaft might not yet be required, potential is unused and improvement is possible. The goal of this thesis is to suggest an approach to improve the overall useful life of the EC225 main rotor shaft, using a combination of the HUMS and RUL estimations. Answering the research question from Section 1.2, the following can be said.

The overall useful life can be increased by maintenance decisions, based on HUMS vibration data for crack diagnostics, the RUL estimations and RCM choices. This research showed how the RUL can be estimated deterministically and what kind of RCM choices can be made based on those RUL estimations. For using the HUMS for crack diagnostics, the possibility of using stiffness change and vibration data is discussed, but the research does not go into more detail.

First of all, crack initiation and propagation can be monitored using the HUMS and vibration data. Based on a changing stiffness, due to crack propagation, the vibration will change. The HUMS monitors the vibration data and detects when, where and how big the crack and crack propagation is. This information can then be used for the RUL estimations.

The HUMS information will indicate a crack in the main rotor shaft. The crack characteristics (SIF's) for this crack are obtained using a finite element model of the main rotor shaft in Abaqus. Using the crack characteristics and the stochastic load input for axial, bending and moment loading, multiple degradation paths are simulated until the point the main rotor shaft will fail, when the SIF reaches K_{Ic}. The degradation paths are then used to create a PDF of the number of flights until failure and the RUL is estimated. It can be seen that higher loading, high variance in loading and a more rough flight, will lead to a lower RUL. Also changing the material of the shaft will influence the RUL drastically.

Based on these RUL estimations, maintenance decisions can be made. These decisions range from basic maintenance planning and inspection interval, to more complicated RCM based decisions. It is shown how the RUL estimations can be implemented into the concept of RCM, taking safety, security and economics into account.

6.1 Limitations

Although this research shows a nice and promising framework to improve the maintenance management using rotor dynamics and fracture mechanics, some limitations need to be pointed out. For clarity, the limitations are divided into different categories: general, loading and crack propagation.

General

This research focuses on the methodology of RUL estimations and maintenance management improvements. The diagnostic part of the research, using HUMS for crack diagnostics, was addressed shortly. Despite the fact that a step-by-step approach is realized, no research is done on the diagnostic part of this approach.

Loading

When looking at the loading input data used for the model, a few limitations need to be discussed. No real-life data was available and therefore assumptions were made to create a stochastic input for the three loading types.

The loading cycles during one flight, the loading sequence, is based on the Felix/28 standard. This leads to the limitation that every flight in this model will have the same basis. No big fluctuations between flights are taken into account. The only variation between flights lies in the stochastic load input using the PDF.

Furthermore, it is assumed that the loading is subdivided into three types, which act on a non-rotating shaft. However, in real life this will not be the case. The shaft is rotating and the loading will act on it differently all the time. In this research, the load is always applied in the same way.

Crack propagation

Assumptions on are made for the crack size, location and direction. In this research an initial horizontal crack of 1 mm is assumed at the second bearing, which will propagate under a constant angle. It is possible that a crack will initiate at a different location and will propagate under a different angle, due to different loading combinations.

In addition, the crack in this research is assumed to be a through crack. However, it is possible that the crack geometry is different. Causing a change in SIF and RUL estimation.

6.2 Future work

This research showed possibilities on how the current maintenance procedure can be improved. However, there are limitations and additional work needs to be done. Next to this, possibilities for future research came to light, discussed in this section. The future work is divided into the different categories as well.

General

First of all, the approach is suggested, elaborated and simulated in this research. However, the model itself is not tested, evaluated and compared with real-life data. This is the first suggestion for future work, validation of the model using real-life input and testing data.

The effect of this approach on maintenance is discussed, more efficient maintenance can be carried out and more potential of the shaft can be used. However, the effect of this approach on for example maintenance costs is not considered. This topic can be seen as a follow up research in the direction of maintenance management, also taking MTTR and MTBF into account.

The framework used and researched in this thesis is focused on one component, the main rotor shaft. Nevertheless, it can also be used and applied to other rotating components or systems. The method stays the same, only the configuration, load case and material change. Future research might look into other applications for this framework.

Loading

Using real-life data as input is a big part of future work. With this data, it is possible to add multiple different flight types, based on probability of occurrence. And it might be possible to use this real-life data to train and improve the model as well.

Crack propagation

It is chosen to focus on the deterministic part of the RUL estimations and maintenance management. The research does not go into detail about the HUMS and how this can be used for diagnostics for cracks and crack propagation. This method should be checked and evaluated as well. Also keeping in mind the minimal detectable crack size.

In this research a relation between the applied loads and the SIF at a certain crack length is found, but still the SIF needs to be determined for every crack length using Abaqus. Future work might look into a relation between the crack length and the SIF,

combining all input variables and improving the model.

The Paris equation is modified to the Walker equation to account for the stress ratio. Other crack growth equations can be used instead and might create results more close to reality. For example the Forman equation, which can be used to fit data that covers both normal and high growth rate regions. Or the Collipriest equation taking all crack growth regions into account.

The SIF threshold value (ΔK_{th}) is not considered during crack propagation calculations. To compensate for this, low stress values in the loading sequence are omitted. In principle, this will have the same result. However, when dealing with real-life data this threshold value needs to be taken into account. This can be done by using for example the Collipriest equation.

The direction of crack propagation is also a point of interest. Due to a change in loading combinations the crack angle might change. Improvement to the model can be achieved, when this change in propagation angle can be taken into account. A possible combination between the computational simulation programs, like NASGRO, Franc3D and AFROW, and the deterministic model is suggested for future work.

As discussed in the limitations, a through crack is considered. The effect of different crack types, like a thumbnail or penny shaped crack, and its influence on the SIF and RUL can be researched.

The degradation level at which the shaft will fail is chosen to be a certain fixed value, the fracture toughness. However, as discussed in Section 3.6, the exact fracture toughness might be unknown or uncertain. An uncertainty for this threshold value can be included in future calculations.

Bibliography

AAIB. **Report on the accident to Eurocopter EC225 LP Super Puma, G-REDU near the Eastern Trough Area Project (ETAP) Central Production Facility Platform in the North Sea on 18 February 2009**. Department for Transport - Air Accidents Investigation Branch, 2011. Available at: https://assets.publishing.service.gov.uk-/media/5422f810ed915d1374000699/1-2011_G-REDU.pdf.

AAIB. **Report on the accidents to Eurocopter EC225 LP Super Puma G-REDW 34 nm east of Aberdeen, Scotland on 10 May 2012 and G-CHCN 32 nm southwest of Sumburgh, Shetland Islands on 22 October 2012**. Department for Transport - Air Accidents Investigation Branch, 2014. Available at: https://assets.publishing.service-.gov.uk/media/5422fbaaed915d1374000833/2-2014_G-REDW_and_G-CHCN.pdf.

AEROSSURANCE. **EC225 main rotor head and Main Gear Box Design**. 2018. Available at: https://aerossurance.com/news/ec225-main-rotor-mgb-design/.

AIBN. **Report on the air accident near Turøy, øygarden municipality, Hordaland County, Norway 29 April 2016 with Airbus helicopters EC225 LP, LN-OJF, operated by CHC helikopter service as**. Accident Investigation Board Norway, 2018. Available at: https://www.sintef.no/globalassets/project/hfc/2018-04-ln-ojf-aibn-2018-rapport-om-luftfartsulykke-nar-turoy-29-april-2016-med-airbus-helicopters-ec-225-lp.pdf.

AIRBUS. **EC225 - Emergency off and rescue from helicopter**. Airbus Helicopters, 2015. Available at: https://www.airbus.com/sites/g/files/jlcbta136/files/2021-10-/225_GRB_E_MC00_A4_VOL01-1.pdf.

AIRBUS. **H225 Technical Information**. 2021. Available at: https://www.airbus.com/en-/products-services/helicopters/civil-helicopters/h225/h225-technical-information.

ANDERSON, T. L. **Fracture Mechanics: Fundamentals and Applications**. [*S.l.*]: Taylor amp; Francis, 2005.

ANTONI, J.; RANDALL, R. B. **The spectral kurtosis: application to the vibratory surveillance and diagnostics of rotating machines**. Mechanical Systems and Signal Processing, v. 20, n. 2, p. 308–331, 2006. ISSN 0888-3270. Available at: https://www.sciencedirect.com/science/article/pii/S0888327004001529.

ATAMURADOV, V.; MEDJAHER, K.; CAMCI, F.; ZERHOUNI, N.; DERSIN, P.; LAMOUREUX, B. **Machine health indicator construction framework for failure diagnostics and Prognostics**. 2020. 591–609 p.

BORDEASU, I.; POPOVICIU, M. O.; MARSAVINA, L.; VODA, M.; NEGRU, R.; PIRVULESCU, L. D. **Numerical simulation of fatigue cracks initiation and propagation for horizontal axial turbines shafts**. Annals of DAAAM Proceedings, 2009.

BOYER, R. R. **Aerospace applications of beta titanium alloys**. JOM, v. 46, p. 20–23, 1994.

COLLIPRIEST, J. **An experimentalist's view of the surface flaw problem**. **The Surface Crack-Physical Problems and Computational Solutions**, ASME, p. 43–61, 1972.

DARLING, D. **Helicopter**. 2016. Available at: https://www.daviddarling.info/encyclopedia/H/helicopter.html.

DOWLING, N. E. **Mechanical behavior of materials: Engineering methods for deformation, fracture, and fatigue**. [*S.l.*]: Pearson Education Limited, 2013.

EASA. **EC225 helicopter accident in Norway - EASA's statement**. European Union Aviation Safety Agency, 2018. Available at: https://www.easa.europa.eu/newsroom-and-events/press-releases/ec225-helicopter-accident-norway-0.

EASA. **Airbus Helicopters Data Sheet: SA 330 / AS 332 / EC 225**. European Union Aviation Safety Agency, 2021. Available at: https://www.easa.europa.eu/downloads/7955/en.

EDWARDS, P.; DARTS, J. Report, **Standardised Fatigue Loading Sequences For Helicopter Rotors (Helix And Felix) - Part 2: Final definition of Helix and Felix**. Farnborough, UK: Royal Aircraft Establishment, 1984.

EUROCOPTER. **M'ARMS / EC225 - EC725 Training Manual**. [*S.l.*]: Eurocopter, 2012.

EVERTS, E. **Internship report: Optimizing the use of gaussian mixture models for the health and usage monitoring system of an EC225 helicopter employing vibrational data**. [*S.l.*]: Instituto Technológico de Aeronáutica - University of Twente, 2016.

FAA. **Metallic Materials Properties Development and Standardization (MMPDS) Handbook – Chapter 5 – Titanium Alloys**. [*S.l.: s.n.*], 2013.

FAA. **Helicopter flying handbook**. [*S.l.*]: Aviation Supplies amp; Academics, Inc., 2019.

FORMAN, R. G.; KEARNEY, V. E.; ENGLE, R. M. **Numerical Analysis of Crack Propagation in Cyclic-Loaded Structures**. Journal of Basic Engineering, v. 89, n. 3, p. 459–463, 09 1967. ISSN 0021-9223. Available at: https://doi.org/10.1115/1.3609637.

FORMAN, R. G.; SHIVAKUMAR, V.; CARDINAL, J. W.; WILLIAMS, L. C.; MCKEIGHAN, P. **Fatigue Crack Growth Database for Damage Tolerance Analysis**. FAA, 2005.

GOODNO, B. J.; GERE, J. M. **Mechanics of Materials**. [*S.l.*]: Cengage Learning, 2012.

GóMEZ, M.; CASTEJóN, C.; GARCíA-PRADA, J. **Crack detection in rotating shafts based on 3 × energy: Analytical and experimental analyses**. Mechanism and Machine Theory, v. 96, p. 94–106, 2016.

HENG, A.; ZHANG, S.; TAN, A. C.; MATHEW, J. **Rotating machinery prognostics: State of the art, challenges and opportunities**. Mechanical Systems and Signal Processing, v. 23, n. 3, p. 724–739, 2009. ISSN 0888-3270. Available at: https://www.sciencedirect.com/science/article/pii/S0888327008001489.

HINES, J. W.; USYNIN, A. **Current Computational Trends in Equipment Prognostics**. 2008. 94-102 p. Available at: https://doi.org/10.2991/ijcis.2008.1.1.7.

KHOO, S. W.; KARUPPANAN, S. **Stress Intensity Factor for Cracks Emanating from a Shaft**. Journal of Applied Sciences, v. 11, 10 2011.

KRAMER, E. **Dynamics of rotors and foundations**. [*S.l.*]: Springer Berlin, 1993.

KUSHWAHA, N.; PATEL, V. N. **Modelling and analysis of a CRACKED ROTOR: A review of the literature and its implications**. Archive of Applied Mechanics, v. 90, n. 6, p. 1215–1245, 2020.

LAND, J. E. **HUMS-the benefits-past, present and future**. 2001 IEEE Aerospace Conference Proceedings (Cat. No.01TH8542), v. 6, p. 3083–3094 vol.6, 2001.

MALIGNO, A.; CHANDWANI, R.; TIMBRELL, C. **NUMERICAL INVESTIGATIONS OF FATIGUE CRACK GROWTH IN SHAFTS**. 2009.

MCCLELLAN, J. M. **Rigid rotorhead MBB BK 117 helicopter**. Feb 2018. Available at: http://www.redbackaviation.com/rigid-rotorhead-mbb-bk-117-helicopter/.

MCCOOL, J. **Using the weibull distribution reliability, modeling, and inference**. [*S.l.*]: John Wiley amp; Sons, 2012.

MIEDLAR, P. C.; BERENS, A. P.; GUNDERSON, A.; GALLANGHER, J. P. **USAF Damage Tolerant Design Handbook: Guidelines for the Analysis and Design of Damage Tolerant Aircraft Structures**. AIR FORCE RESEARCH LABORATORY, 2002. Available at: https://apps.dtic.mil/sti/pdfs/ADA411872.pdf.

NASA. **NASA Reliability-Centered Maintenance guide**. [*S.l.: s.n.*], 2008.

OLIVEIRA, M. C. C. Z. de. Master Thesis, **Aircraft structural inspections definition considering probabilistic analysis of failures based on variability of crack growth parameters and probability of detection**. [*S.l.*]: Instituto Technológico de Aeronáutica, 2018.

PARIS, P. C.; GOMEZ, M. P.; ANDERSON, W. E. **A rational analytic theory of fatigue**. The Trend in Engineering, v. 13, p. 9–14, 1961.

PRASAD, S. R.; SEKHAR, A. S. **Detection of fatigue crack in the shaft using time-frequency analysis**. Lecture Notes in Mechanical Engineering, p. 433–443, 2020.

PRENSCIA, H. **Characteristics of the Weibull distribution**. Reliability HotWire, 2001. Available at: https://www.weibull.com/hotwire/issue14/relbasics14.htm.

PRIDE, A. **Reliability-Centered Maintenance (RCM)**. Sep 2016. Available at: https://www.wbdg.org/resources/reliability-centered-maintenance-rcm.

RANDALL, R. B. **Vibration-based condition monitoring: Industrial, aerospace and Automotive Applications**. [*S.l.*]: John Wiley amp; Sons, 2011.

RAYCHAUDHURI, S. **Introduction to monte carlo simulation**. 2008 Winter Simulation Conference, 2008.

SAJITH, S.; MURTHY, K. K.; ROBI, P. **Fatigue life prediction under mixed-mode loading using equivalent stress intensity factor models**. MATEC Web of Conferences, v. 172, 2018.

SCHONENBERG, W. **Internship report: Improving the HUMS Capabilities of an EC225 Helicopter by Training a Model for Automatic Failure Detection of an Oil Cooler Fan Shaft**. [*S.l.*]: Instituto Technológico de Aeronáutica - University of Twente, 2015.

SEAFORCES. **EC225 Super Puma / EC725 Caracal**. Seaforces - online, 1999. Available at: https://www.seaforces.org/marint/French-Navy/AVIATION/EC225-Super-Puma.htm.

SEIDENMAN, P. **HUMS: Not just for heavy iron anymore**. Jul 2020. Available at: https://rotormedia.com/hums/.

SILVA, A.; ZARZO, A.; GONZáLEZ, J. M. M.; MUNOZ-GUIJOSA, J. M. **Early fault detection of single-point rub in gas turbines with accelerometers on the casing based on continuous wavelet transform**. Journal of Sound and Vibration, v. 487, p. 115628, 2020.

SIMULIA. **11.4.2 Contour integral evaluation**. 2006. Available at: https://classes.engineering.wustl.edu/2009/spring/mase5513/abaqus/docs/v6.6/books-/usb/default.htm?startat=pt04ch11s04aus57.html.

SKYBRARY. **Health and Usage Monitoring System (HUMS)**. SKYbrary, n.d. Available at: https://www.skybrary.aero/articles/health-and-usage-monitoring-system-hums.

TEYI, N.; SINGH, S. **A decadal review of various modelling and analysis of cracked rotors**. Procedia Structural Integrity, v. 39, p. 333–346, 2022.

TINGA, T. Application of physical failure models to enable usage and load based maintenance. **Reliability Engineering amp; System Safety**, v. 95, n. 10, p. 1061–1075, 2010.

TINGA, T. **Principles of loads and failure mechanisms applications in maintenance, reliability and Design**. [*S.l.*]: Springer London, 2013.

UNDERWOOD, J. H.; FORMAN, R. G.; SHIVAKUMAR, V. **Growth Behavior of Surface Cracks in the Circumferential Plane of Solid and Hollow Cylinders**. *In*: _____. **Fracture Mechanics: Seventeenth Volume: Seventeenth national symposium on fracture mechanics**. [*S.l.*]: ASTM, 1986. p. 59–74.

USYNIN, A.; HINES, J. W.; URMANOV, A. **Uncertain failure thresholds in cumulative damage models**. 2008. 334-340 p.

WALKER, K. **The Effect of Stress Ratio During Crack Propagation and Fatigue for 2024-T3 and 7075-T6 Aluminum**. **Effects of Environment and Complex Load History on Fatigue Life**, ASTM International, p. 1–14, 1970. Available at: https://doi.org/10.1520/STP32032S.

WIIG, J. **Optimization of fault diagnosis in helicopter health and usage monitoring systems**. ENSAM, 2006.

YANG, Y.; VORMWALD, M. **Fatigue crack growth simulation under cyclic non-proportional mixed mode loading**. International Journal of Fatigue, v. 102, p. 37–47, 2017. Available at: https://www.sciencedirect.com/science/article/pii/S0142112317301950.

ZHANG, X. Q.; WANG, J.; WEI, W.; JI, X. T.; CHEN, B.; FANG, G. W. **Simulation of fatigue cracks growth processes of two parallel cracks in thin plate pulled by the constant amplitude cyclic loading**. Journal of the Brazilian Society of Mechanical Sciences and Engineering, v. 41, n. 9, 2019.

ZHAO, F.; TIAN, Z.; BECHHOEFER, E.; ZENG, Y. **An integrated prognostics method under time-varying operating conditions**. IEEE Transactions on Reliability, v. 64, n. 2, p. 673–686, 2015.

ZHU, J.; NOSTRAND, T.; SPIEGEL, C.; MORTON, B. **Survey of condition indicators for condition monitoring systems**. 01 2014. 635-647 p.

ZIPAY, J. J.; MODLIN, C. T.; LARSEN, C. E. **The ultimate factor of safety for aircraft and spacecraft - its history, applications and misconceptions**. 57th AIAA/ASCE/AHS/ASC Structures, Structural Dynamics, and Materials Conference, 2016.

Appendix A - Walker equation constants for Titanium Ti-6Al-4V

In this appendix approximate values are obtained for the Walker equation constants C_0, m and γ for Ti-6Al-4V. These approximated are based on procedures discussed by Downling (DOWLING, 2013). For these calculations the Fatigue-crack-propagation data for Ti-6Al-4V is used, shown in Figure A.1.

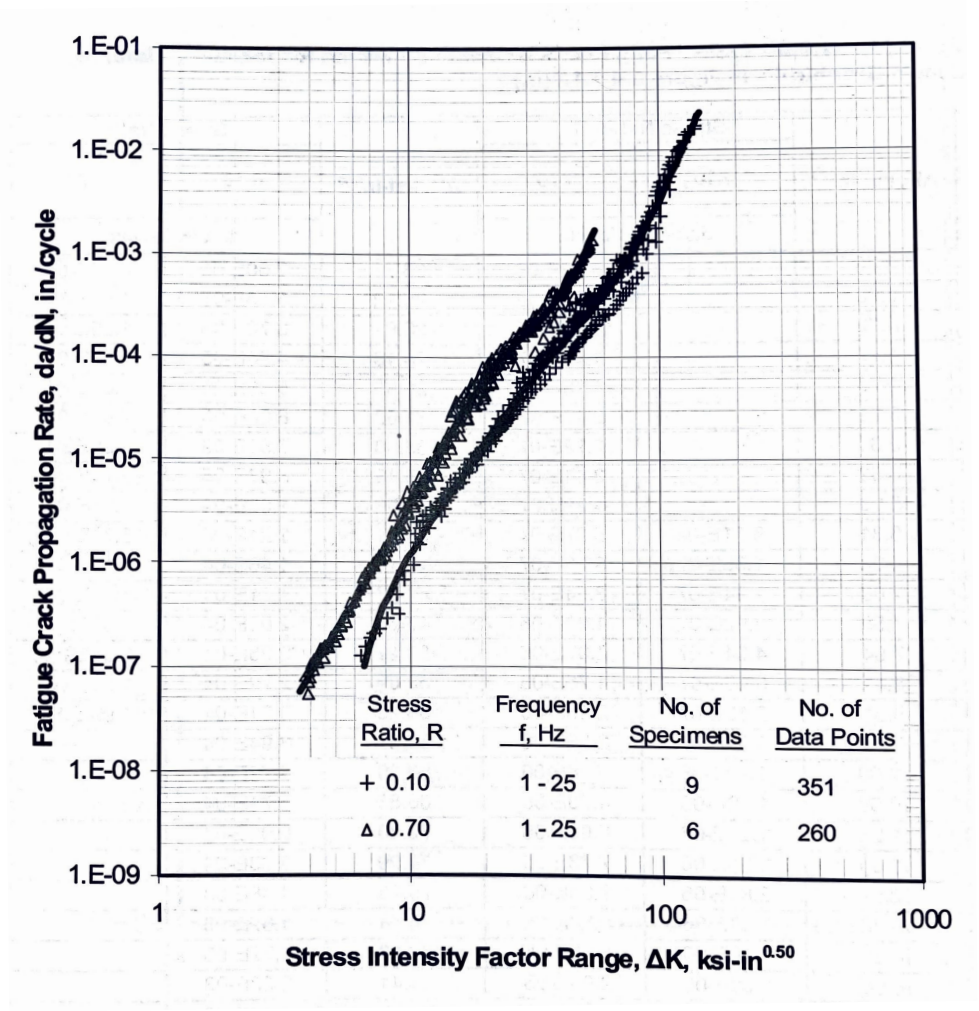

FIGURE A.1 – Fatigue-crack-propagation data for Ti-6Al-4V titanium alloy (FAA, 2013)

This figure shows the relation between the crack growth rate and stress intensity range for two values of the stress ratio R, for $R = 0.10$ and $R = 0.70$. Equation 3.1 is used to

determine C_0, m and γ:

$$\frac{da}{dN} = C(\Delta K)^m \tag{A.1}$$

Together with:

$$C = \frac{C_0}{(1-R)^{m(1-\gamma)}} \tag{A.2}$$

First, the data for R = 0.10 is used to determine situation specific C and m values:

The data falls along a straight line, that passes two points, $(\Delta K,\ \frac{da}{dN})$:

$$A:\ (9,\ 1*10^{-6}) \quad \text{and} \quad B:\ (70,\ 8*10^{-4}) \quad (ksi\sqrt{in},\ in/cycle)$$

Converting to SI-units:

$$A:\ (9.890,\ 2.54*10^{-5}) \quad \text{and} \quad B:\ (76.919,\ 2.032*10^{-2}) \quad (MPa\sqrt{m},\ mm/cycle)$$

Equation A.1 and the two points give:

$$\frac{da}{dN}_A = C(\Delta K_A)^m \qquad \frac{da}{dN}_B = C(\Delta K_B)^m \tag{A.3}$$

$$\frac{da/dN_A}{da/dN_B} = \left(\frac{\Delta K_A}{\Delta K_B}\right)^m \tag{A.4}$$

Solving for m:

$$m = \frac{\log(da/dN_A) - \log(da/dN_B)}{\log(\Delta K_A) - \log(\Delta K_B)} = \frac{\log(2.54*10^{-5}) - \log(2.032*10^{-2})}{\log(9.890) - \log(76.919)} = 3.259 \tag{A.5}$$

Now the C parameter can be obtained by substituting m into Equation A.1:

$$2.54*10^{-5} = C(9.890)^{3.259}, \quad C = 1.450*10^{-8}\ \frac{mm/cycle}{MPa\sqrt{m}} \tag{A.6}$$

So for the $R = 0.10$ case the line can be described by:

$$\frac{da}{dN} = 1.450*10^{-8}(\Delta K)^{3.259} \tag{A.7}$$

Now the same is done for the $R = 0.70$ case. The data is roughly parallel to the $R = 0.10$ data, so the same $m = 3.259$ is used. The data goes through point:

$$(10,\ 4*10^{-6}) \quad (ksi\sqrt{in},\ in/cycle)$$

Converting to SI-units:

$$(10.988,\ 1.016 * 10^{-4}) \quad (MPa\sqrt{m},\ mm/cycle)$$

For this second case, the C can be found by substituting these values and $m = 3.259$ into Equation A.1:

$$1.016 * 10^{-4} = C(10.988)^{3.259}, \quad C = 4.117 * 10^{-8}\ \frac{mm/cycle}{MPa\sqrt{m}} \tag{A.8}$$

So for the $R = 0.70$ case the line can be described by:

$$\frac{da}{dN} = 4.117 * 10^{-8}(\Delta K)^{3.259} \tag{A.9}$$

Two values of C are obtained for both R. Those values must meet the relation given in Equation A.2:

$$C_{0.10} = \frac{C_0}{(1-R)^{m(1-\gamma)}}, \quad C_{0.70} = \frac{C_0}{(1-R)^{m(1-\gamma)}} \tag{A.10}$$

Substituting all parameters, C, R and m, will give two equations with two unknowns, the C_0 and the γ:

$$1.450 * 10^{-8} = \frac{C_0}{(1-0.10)^{3.259(1-\gamma)}}, \quad 4.117 * 10^{-8} = \frac{C_0}{(1-0.70)^{3.259(1-\gamma)}} \tag{A.11}$$

Combining the two equations and solving it gives:

$$\log \frac{1.450 * 10^{-8}}{4.117 * 10^{-8}} = 3.259(1-\gamma) \log \frac{0.3}{0.9}, \quad \gamma = 0.709 \tag{A.12}$$

Now the C_0 is found by substituting this γ into A.11:

$$C_0 = \frac{1.450 * 10^{-8}}{(1-0.10)^{3.259(1-0.709)}} = 1.602 * 10^{-8}\ \frac{mm/cycle}{MPa\sqrt{m}} \tag{A.13}$$

Concluding, the walker parameters for Ti-6Al-4V are $C_0 = 1.602 * 10^{-8}\ \frac{mm/cycle}{MPa\sqrt{m}}$, $m = 3.259$ and $\gamma = 0.709$.

Appendix B - Load diagrams

B.1 Load diagram: Axial load

Because of a reaction force of the rotors carrying the helicopter an axial force is present. This axial force creates a tension throughout the shaft, which will be evenly spread. This is shown in Figure B.1.

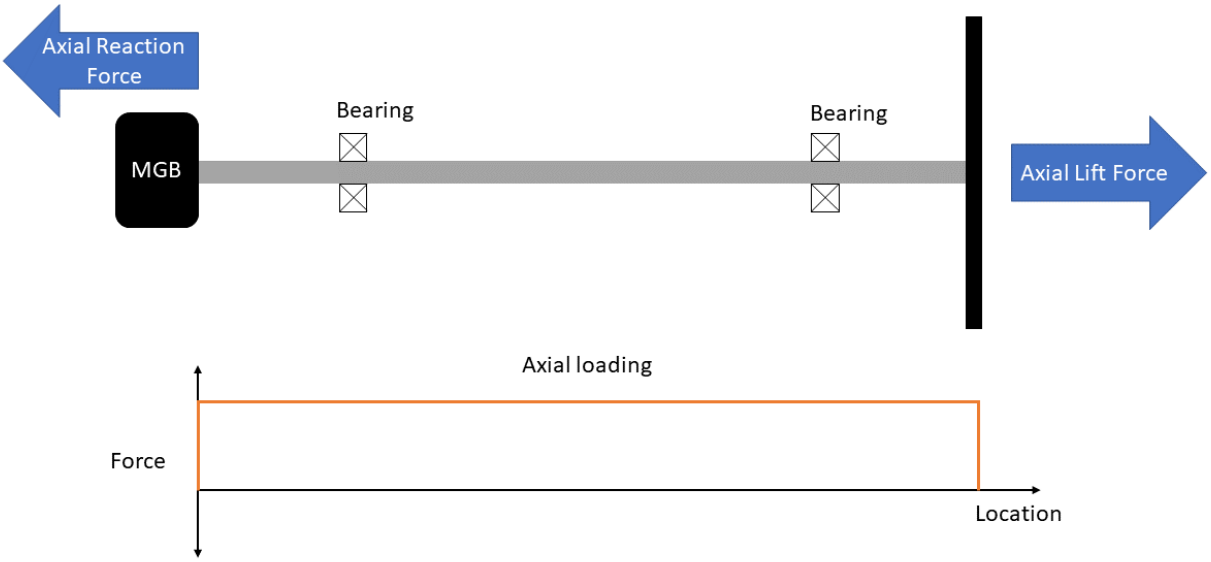

FIGURE B.1 – Load diagram for axial loading

B.2 Load diagram: Bending load

For different reasons or circumstances there can be a radial force (bending) acting on the shaft at the rotor location, think about wind, movement, environment, etc. This radial force will lead to a shear and bending moment in the shaft, shown in Figure B.2. It can be seen that the shear is highest in the last part, between the last bearing and the rotor. And the bending moment will be highest at the last bearing. The load (or local stress) will therefore be highest just after the second bearing, and cracking is most likely to happen here.

Equilibrium:

$$\sum F = 0 \qquad \text{(B.1)}$$
$$-F_A + F_B - F_R = 0$$

$$\sum M = 0 \qquad \text{(B.2)}$$
$$L_1 F_B - (L_1 + L_2) F_R = 0$$

Gives:

$$F_B = F_R(L_1 + L_2)/L_1 \qquad \text{(B.3)}$$
$$F_A = F_R(L_2/L_1)$$

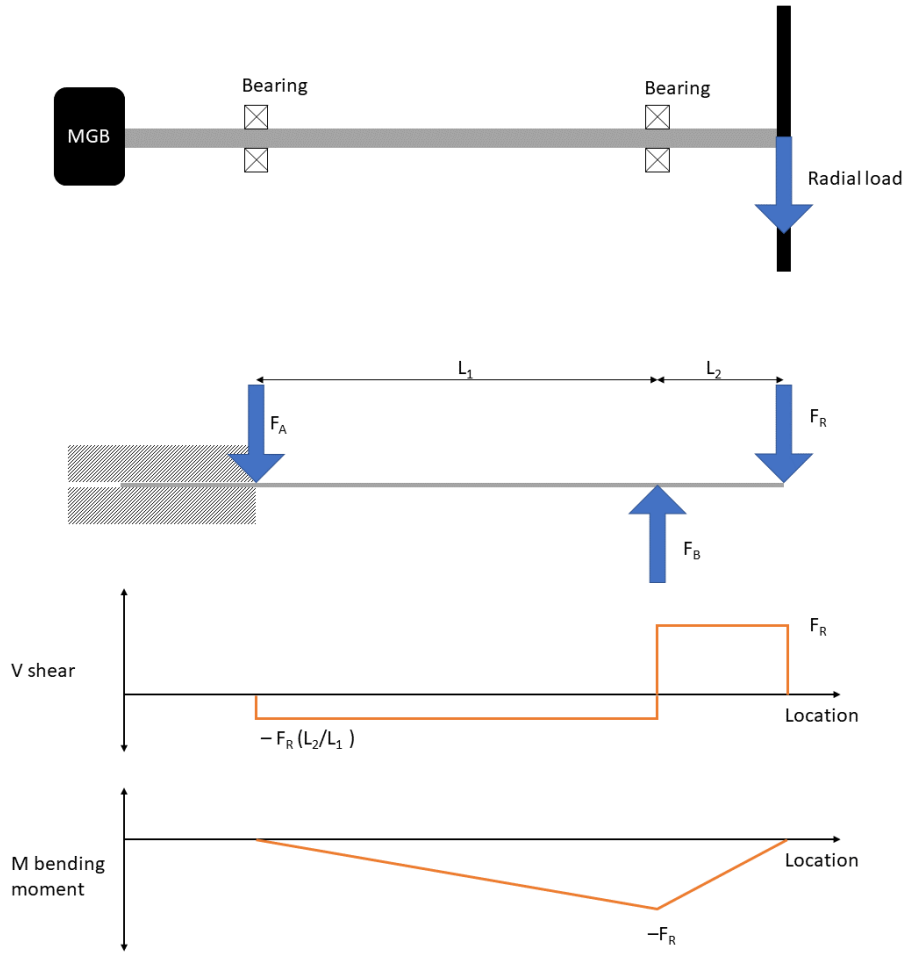

FIGURE B.2 – Load diagram for bending

B.3 Load diagram: Moment load

The MGB uses the main rotor shaft to transfer the appropriate torque to the main rotors. This can and will cause a moment that is present in the main rotor shaft. In Figure B.3 a schematic representation is shown. It is possible that certain influences on for example the blades causes loading peaks. However, the torque (and therewith possible shear) is distributed over the whole shaft. So in this case no real load concentration is present.

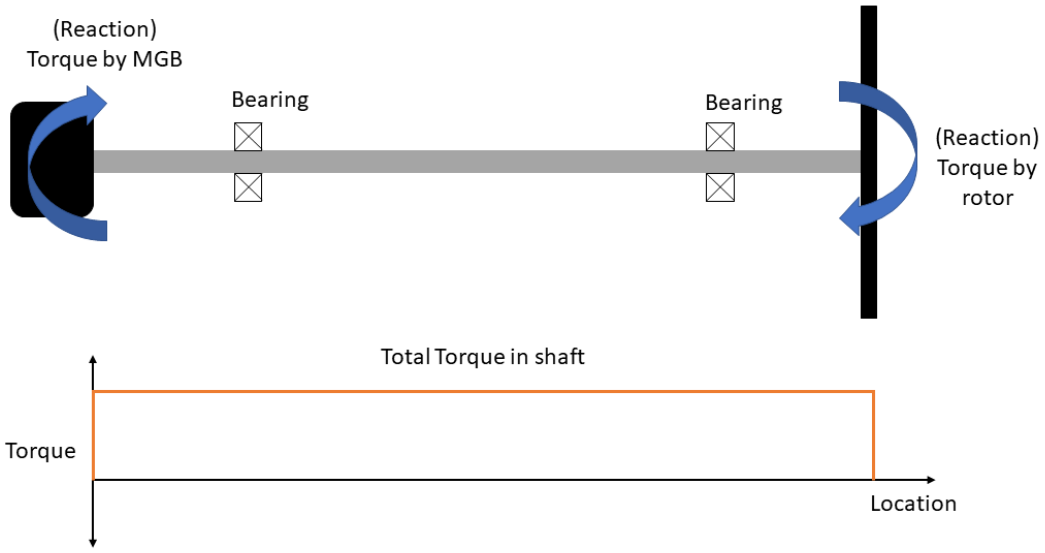

FIGURE B.3 – Load diagram for moment

Appendix C - Felix standard for loading sequence

The Felix standard from 1984 (EDWARDS; DARTS, 1984) is extensive and the loading scenarios are divided into types of flight, with different duration and with different manoeuvres. Therefore, some simplifications have been made for this research and the model. Because for some manoeuvres the amplitude of the cycle is relatively small compared to the big loading cycles, small loading cycles are omitted. The levels of omission for normal use are chosen by the standard to be 28 for Felix, which is addressed as Felix/28. Following the Felix/28 standard, a loading sequence based on defined manoeuvres is created and shown in Table C.1. In the first column the manoeuvres are shown. In the second column the mean loading and the amplitude of the cycle is given, in which the cycle goes positive first.

TABLE C.1 – Sequence of loads for each manoeuvre based on Felix/28 (EDWARDS; DARTS, 1984)

Manoeuvre	**Mean load – amplitude of every cycle (positive first)**
Take off	32 - 28 28 28 28 28 28 28 28 28 32 28 28
Forward flight (at different speeds)	48 - 24 16 24
Transition to hover	40 - 24
Hover	36 - 24
Cruise turns 1	60 - 24
Cruise turns 2	64 - 28
Sideways flight port	36 - 24
Sideways flight starboard	36 - 28 28 28 28 28 28 32 28 28 28 28 28 28 28
Rearwards flight	36 - 28
Spot turns	36 - 24
Autorotation	40 - 32 28 32 28 28 36 28 28 44 28 28 28 32 28
Recoveries from autorotation	36 - 24
Control reversals 1	36 - 28 28 36 32 28 32 32 28 28
Control reversals 2	44 - 36 32 28 36 32 28 28 28 28 32
Descent	36 - 28 28 28 28 28 28 28 32 28 28 28 28 28 28 28 28 28 28 28 28 28 32 28 28 28 28 28 28
Landing	8 - 36 36

In the standard the loading is given in Felix-units. This unit is dimensionless and is used to represent loads or strains on a scale up to 100, with intervals of 4. In this research the load will be expressed on a scale up to 100 as well, in which 100 is the maximum possible load. This loading sequence data for one flight is displayed in a graph in Figure 4.6.

Appendix D - Mathematical explanation: Load change and SIF

As explained in Section 4.3.1, the SIF at the crack for a combination of loads can be determined using the ratio between a chosen load and the baseline load and using superposition. This principle is explained in more detail in this Appendix.

In the model three loading types are considered: (1) Axial loading; (2) Bending; (3) Moment or torque. For each type of loading the SIF is obtained at a certain baseline load. At a baseline loading of 1000 N or Nmm and a crack size of 1 mm the following values for K_I and K_{II} are obtained using Abaqus:

TABLE D.1 – SIF's at baseline load of 1000 N for axial and bending and 1000 Nmm moment loading

	Axial		Bending		Moment	
	K_I	K_{II}	K_I	K_{II}	K_I	K_{II}
SIF	0.642	0.000	4.231	-0.004	0.000	-0.011

Next, these SIF can be multiplied by the ratio between the load of interest and the baseline load. The loads of interest are: Axial = 1.1e5 N, Bending = 5.5e4 N and Moment = 2.4e6 Nmm. Multiplying the SIF's from Table D.1 with the ratio gives the following:

TABLE D.2 – SIF's at load of interest for axial, bending and moment loading

	Axial (1.1e5 N)		Bending (5.5e4 N)		Moment (2.4e6 Nmm)	
	K_I	K_{II}	K_I	K_{II}	K_I	K_{II}
SIF	70.565	-0.018	232.705	-0.207	-0.003	-25.574

Now that the K_I and K_{II} values per load are know, superposition can be used to obtain values for K_I and K_{II} at a combination of these loads. The results of this superposition are given in Table D.3. To validate these results, the SIF's for this combination of loads are also computed with Abaqus. These results are also shown in Table D.3.

TABLE D.3 – Comparison of calculated K_I and K_{II} values and Abaqus results

	K_I	K_{II}
SIF	303.27	-25.80
Abaqus	303.3	-25.80

It can be seen that the SIF's computed using the ratio's and superposition are almost the same as the values from Abaqus. Therefore, it is assumed that this principle can be used for the SIF calculations.

Appendix E - Abaqus output

For a baseline loading of 1000 N or Nmm for axial, bending and moment load, the SIF are determined using Abaqus. This is the main data that is obtained using the finite element software. The results are shown in Table E.1. In the first column the crack length is shown. The rest of the columns is divided into three main parts, the loading types. For each loading a division is made for the SIF mode I or II (K1 and K2) and the crack side (C1 and C2). Also for AISI 4340 stainless steel the Abaqus output is obtained and shown in Table E.2.

TABLE E.1 – SIF's for every crack length $[mm]$ per baseline load for mode I or II (K1 and K2) and both crack sides (C1 and C2) [MPa/$\sqrt{mm}$] for Ti-6Al-4V

	Axial				**Bending**				**Moment**			
Crack Length	**K1C1**	**K2C1**	**K1C2**	**K2C2**	**K1C1**	**K2C1**	**K1C2**	**K2C2**	**K1C1**	**K2C1**	**K1C2**	**K2C2**
1	0.6415	-0.0002	0.6418	0.0001	4.2310	-0.0038	4.2330	0.0031	0.0000	-0.0107	0.0000	-0.0107
3	1.0500	0.0800	1.0500	0.0800	7.0000	0.5000	7.0000	0.5000	0.0040	-0.0170	0.0040	-0.0170
7	1.6680	0.1677	1.6700	0.1699	11.0000	1.0780	10.9800	1.1490	0.0090	-0.0261	0.0090	-0.0261
10	2.0000	0.1917	2.0040	0.1911	13.1800	1.2300	13.1500	1.3200	0.0109	-0.0308	0.0109	-0.0308
20	2.8930	0.2613	2.8920	0.2670	18.9500	1.6910	18.8000	1.9940	0.0151	-0.0419	0.0150	-0.0419
30	3.6500	0.3506	3.6380	0.3594	23.6600	2.3000	23.3300	2.8780	0.0177	-0.0517	0.0177	-0.0516
40	4.3930	0.4294	4.3690	0.4459	28.0700	2.8510	27.5400	3.8160	0.0201	-0.0620	0.0200	-0.0619
50	5.1660	0.4798	5.1220	0.5099	32.4100	3.2290	31.6200	4.6960	0.0226	-0.0736	0.0223	-0.0735

TABLE E.2 – SIF's for every crack length $[mm]$ per baseline load for mode I or II (K1 and K2) and both crack sides (C1 and C2) [MPa/$\sqrt{mm}$] for AISI 4340 stainless steel

	Axial				**Bending**				**Moment**			
Crack Length	**K1C1**	**K2C1**	**K1C2**	**K2C2**	**K1C1**	**K2C1**	**K1C2**	**K2C2**	**K1C1**	**K2C1**	**K1C2**	**K2C2**
1	0.6406	-0.0002	0.6409	0.0001	4.2290	-0.0038	4.2310	0.0031	0.0000	-0.0106	0.0000	-0.0106
3	1.0500	0.0800	1.0500	0.0800	7.0000	0.5000	7.0000	0.5000	0.0040	-0.0170	0.0040	-0.0170
7	1.6610	0.1780	1.6630	0.1800	10.9700	1.1480	10.9500	1.2190	0.0090	-0.0261	0.0090	-0.0261
10	1.9910	0.2031	1.9950	0.2020	13.1300	1.3080	13.1100	1.3950	0.0108	-0.0307	0.0109	-0.0307
20	2.8830	0.2697	2.8750	0.2775	18.9000	1.7560	18.7100	2.0410	0.0150	-0.0417	0.0150	-0.0418
30	3.6400	0.3515	3.6280	0.3637	23.6100	2.3250	23.2900	2.9260	0.0176	-0.0514	0.0175	-0.0514
40	4.3850	0.4210	4.3520	0.4424	28.0400	2.8260	27.4500	3.8190	0.0200	-0.0617	0.0198	-0.0617
50	5.1630	0.4662	5.1160	0.5019	32.4100	3.1800	31.6000	4.6770	0.0224	-0.0734	0.0221	-0.0732

Appendix F - Monte Carlo simulation iterations

When using the Monte Carlo method, it is important to know how many iterations are needed. Too few iterations will cause the accuracy to be low, and too many iterations will cause the model to run forever. Because there is no experimental data available, it is not possible to validate the number of iterations statistically.

To overcome this problem, multiple number of iterations are tested and the results are compared. The result of these different number of iterations are shown in Figure F.1. In this Figure the RUL and the standard deviation is plotted against the number of iterations. The RUL is calculated using Equation 5.1 and the standard deviation is calculated using the following equation (MCCOOL, 2012):

$$\sigma = \eta * \sqrt{\Gamma\left(\frac{2}{\beta}+1\right) - \Gamma\left(\frac{1}{\beta}+1\right)^2} \tag{F.1}$$

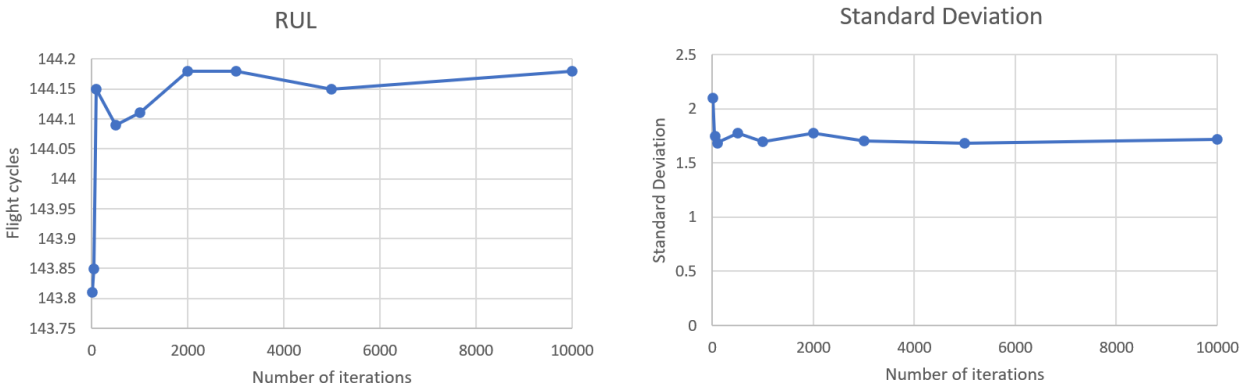

(a) (b)

FIGURE F.1 – RUL (a) and Standard Deviation (b) results from the model for different number of iterations

It can be seen that after 2000 iterations the difference between results of consecutive number of iterations is small, the line in both graphs flattens out. Because of this small difference between 2000 and more iterations, it is assumed that 2000 iterations is sufficiently accurate to use for the model. More iterations is possible, but the time to run the model increases fast. A simulation with 10 000 takes for example half a day to run.

FOLHA DE REGISTRO DO DOCUMENTO

1. CLASSIFICAÇÃO/TIPO	2. DATA	3. DOCUMENTO Nº	4. Nº DE PÁGINAS
DM	21 de março de 2023	DCTA/ITA/DM-.../2023	78

5. TÍTULO E SUBTÍTULO:
Remaining useful life estimation framework for maintenance improvement of a helicopter main rotor shaft using fracture mechanics

6. AUTOR(ES):
Samuel Franciscus Zijp

7. INSTITUIÇÃO(ÕES)/ÓRGÃO(S) INTERNO(S)/DIVISÃO(ÕES):
Instituto Tecnológico de Aeronáutica – ITA & University of Twente – UT

8. PALAVRAS-CHAVE SUGERIDAS PELO AUTOR:
Remaining useful life; Aircraft maintenance; Fracture mechanics; Helicopter main rotor shaft; Crack propagation

9. PALAVRAS-CHAVE RESULTANTES DE INDEXAÇÃO:
Vida útil remanescente; Manutenção de aeronaves; Mecânica da fratura; Rotor principal de helicópter; Propagação da trinca

10. APRESENTAÇÃO: ( ) **Nacional** (**X**) **Internacional**
ITA, São José dos Campos. Curso de Mestrado. Programa de Pós-Graduação em Engenharia Aeronáutica e Mecânica. Area of Aeronautical Design, Aerospace Systems and Structures. Orientador: Prof. Dr. Airton Nabarrete. Coorientadora: Dr. Alberto Martinetti (UT). Defesa em 21/03/2023. Publicada em 21/03/2023.

11. RESUMO:
This research aims to make the next step from diagnostics towards prognostics, using the Health and Usage Monitoring System (HUMS) in combination with fracture mechanics to determine the Remaining Useful Life (RUL) of a helicopter main rotor shaft. This main rotor shaft transfers the power delivered by the engine and the main gear box to the main rotors. At the moment, maintenance to this shaft is carried out after a fixed amount of time, resulting in unused potential. The RUL predictions are used to improve this maintenance strategy and are based on the crack propagation of the main rotor shaft. A framework for these RUL estimations is created using a combination of stochastic, deterministic and statistical calculations. Three main loading types are used as input for the crack propagation calculations: axial, bending and moment loading. Probability density functions (PDF) of these loads are created and used as stochastic load input. A relation is found between the load, crack geometry and stress intensity factor (SIF). This SIF is obtained by modeling the cracked main rotor shaft in the finite element program Abaqus. The relation between the load, crack geometry and SIF is then used to calculate the crack growth rate deterministically using the Walker modification on the Paris' law and Irwin's model. The crack growth rate is calculated for different stress levels during flights. Each flight consists of different stress levels, based on the Felix/28 standard in combination with the PDF stochastic load input. Using this crack growth rate, the crack propagation during flights is determined and so-called degradation paths are constructed. Using the Monte Carlo method, multiple degradation paths are simulated and the RUL is estimated statistically. At last, this RUL estimation is used for maintenance purposes, like determining the inspection interval and plan and anticipate maintenance scenarios. But also putting this framework into the bigger picture of Reliability-Centered Maintenance (RCM).

12. GRAU DE SIGILO:
(**X**) **OSTENSIVO** ( ) **RESERVADO** ( ) **SECRETO**